NACA TN 3472

NATIONAL ADVISORY COMMITTEE FOR AERONAUTICS

TECHNICAL NOTE 3472

FLOW STUDIES ON FLAT-PLATE DELTA WINGS AT SUPERSONIC SPEED

By William H. Michael, Jr.

Langley Aeronautical Laboratory
Langley Field, Va.

Washington
July 1955

NATIONAL ADVISORY COMMITTEE FOR AERONAUTICS

TECHNICAL NOTE 3472

FLOW STUDIES ON FLAT-PLATE DELTA WINGS AT SUPERSONIC SPEED

By William H. Michael, Jr.

SUMMARY

An experimental study has been made to investigate some aspects of the nature of the flow around delta wings. Vapor-screen, pressure-distribution, and ink-flow studies were made at a Mach number of 1.9 on a series of semispan delta-wing models with slender wedge airfoil sections and very sharp leading edges. The models had semiapex angles ranging from 5° to 31.75°.

Separated regions of vorticity existed along the chords of all the wings in the series tested. Concentrated vortex cores were found only on wings of very small semiapex angles. For wings with medium and large semiapex angles, the separated vorticity was concentrated in a region extending over the outboard part of the span and lying close to the wing upper surface.

The results show that theoretical aerodynamic calculations, such as those in NACA TN 3430, utilizing a single, separated vortex pair above the wing upper surface to represent the separated vorticity can be applied at supersonic speeds for very slender wings.

INTRODUCTION

Theoretical calculations of aerodynamic phenomena usually require some basic assumption concerning the physical nature of the flow field. In calculations of the velocity fields behind wings, for instance, the vorticity is for some cases assumed to be concentrated in a vortex sheet and for others to be concentrated in discrete vortices, the choice depending on the wing aspect ratio, lift coefficient, distance from the trailing edge, and other factors. (See ref. 1, for instance.) The vortex sheets and discrete vortices have usually been assumed to leave the wing at the trailing edge. In a recent attempt to predict theoretically the lift on slender delta wings (ref. 2), separation was assumed to take place from the leading edges of the wings. For that analysis,

then, the vortex sheet was assumed to roll up into discrete vortices lying above the wing and increasing in strength along the chord of the wing.

Since the latter assumptions differ considerably from most of those used in past analyses, an experimental investigation of the flow phenomena was proposed. The purpose of the present study is to investigate aspects of the physical nature of the flow field along the chords of a series of small- and medium-aspect-ratio delta wings. This investigation is of a qualitative nature and serves primarily to define the vortex-separation phenomena and to indicate a general range of applicability of the separated-vortex concept.

SYMBOLS

α	angle of attack, deg
ϵ	wing semiapex angle, deg
$b/2$	wing semispan, in.
M	Mach number
$\frac{\Delta p}{q}$	pressure coefficient, $\frac{p_l - p}{q}$
p_l	local static pressure
p	free-stream static pressure
q	free-stream dynamic pressure
μ	Mach angle, $\sin^{-1}\frac{1}{M}$
y	spanwise coordinate, in.

APPARATUS AND MODELS

The tests for this investigation were made in a 9- by 6-inch, Mach number 1.9 blowdown jet of the Langley gas dynamics laboratory. The test section was equipped with a boundary-layer scoop-off plate to minimize the effect of boundary layer on the essentially flat-plate semispan models. (See fig. 1.) With this boundary-layer scoop-off plate, the maximum boundary-layer thickness was calculated to be about 3 percent

of the span for the wing with the smallest span. The present tests were made at a Reynolds number of 1.58×10^6 per inch.

A vapor-screen technique similar to that used in reference 3 was used in the present tests to observe the flow phenomena around delta wings. In this technique, water was inserted in the air-supply line upstream of the settling chamber. After the water was broken into very small droplets by the settling-chamber turbulence screens and expanded through the nozzle, it appeared in the test section as a fog. A mercury-vapor light source was used to produce a narrow slit of intense light perpendicular to the tunnel axis. (See fig. 2.) The light scattered by the particles appeared as a screen of illumination on which changes of density showed up as changes in intensity of illumination (see appendix); therefore, regions of concentrated vorticity and shock waves could be observed. An aerial camera was used to take photographs of the vapor screen. The change in Mach number with the addition of water was found by static-pressure measurements to be small ($\Delta M = -0.03$) with respect to the Mach number obtained without water addition.

The models used in this investigation were essentially flat-plate semispan delta-wing models with slender wedge airfoil sections and very sharp leading edges. The maximum thickness of the wings was of the order of 1.7 to 4.4 percent of the chord. Models with semiapex angles of 5°, 7.5°, 10°, 15°, 22.5°, and 31.75° were tested. Dimensions of the models are given in figure 3.

For the pressure-distribution tests, pressure orifices were installed on one surface of the models, and the models were tested at positive and negative angles of attack to determine the pressure on both the upper and lower surfaces.

The pressure orifices were also used for ink-flow studies. For these studies, ink was inserted through several of the pressure orifices under sufficient pressure to obtain a steady flow of ink over the surface of the wing.

TESTS AND RESULTS

Vapor-screen tests were made at two chordwise positions for each wing model of the series, and the photographs of these results are presented in figures 4 to 9. The flow phenomena observed over the wing appeared to be steady. These photographs were taken from a position outside the tunnel and at an angle with the tunnel axis; thus the vortex cores do not appear in the photographs at their true distance above the wing surface, although the spanwise positions are correctly represented. The actual distance of the apparent vortex cores above the wing surface

can be obtained from the camera angle and wing angle of attack. For these photographs, the actual distances above the wing surface are of the order of twice the observed distances because the camera angle is approximately 60°.

Pressure distributions at one chordwise position for each model are presented in figures 10 to 15. For some wings, pressure distributions were obtained at other chordwise positions, but these were essentially the same as those presented and, therefore, are not given.

The ink-flow test results are presented in figures 16 to 21. The wings were painted white for these tests to give better contrast between the light and dark regions.

DISCUSSION

The vapor-screen photographs are essentially self-explanatory, but some of the more important aspects of the photographs should be noted. The dark regions in the photographs correspond to regions of low density; hence, they show less reflection from the particles in the airstream than do the surrounding regions. (See appendix.) In various photographs the dark regions may indicate concentrated vortex cores, regions of separated flow, or low-density regions preceding shock waves.

The primary interest in the pressure distributions is in the conditions on the suction or upper surfaces of the wings. Ink-flow studies were included in the present tests to give an indication of the flow characteristics in the boundary layer.

Wings With Semiapex Angles of 5°, 7.5°, and 10°

For the wings with the smallest semiapex angles, the vortex cores are well defined and lie well above the wing surfaces. With an increase in the semiapex angle ϵ, the vortex cores become larger and remain closer to the wing upper surfaces. (See figs. 4 to 6.) The effects of increasing the angle of attack are that the vortex cores increase in size, move inboard, and extend a greater distance above the wing surface. The general conical nature of the flow is indicated by the similarity of the vapor-screen photographs at the two chordwise positions considered for each wing.

The upper-surface pressure distributions in figures 10 to 12 show gradual spanwise decreases in pressure toward negative pressure peaks which are situated at the same spanwise positions as the vortex cores. Some comparisons of the measured pressure distributions with the calculated distributions are given in a subsequent section.

The ink-flow photographs (figs. 16 to 18) show an outward movement of ink toward the leading edge, which indicates a flow separation at the leading edge, and an ink accumulation along a line inboard of the leading edge but outboard of the vortex-core position. A suggested explanation of the phenomena in the boundary layer is given with the aid of the accompanying sketch which is a section taken normal to the main stream at a particular chordwise position.

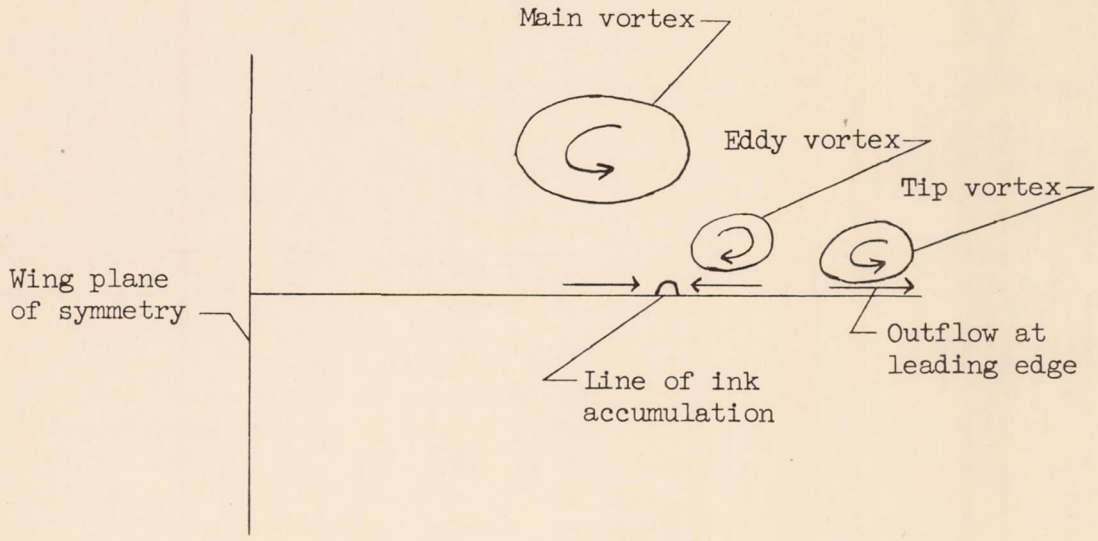

The observed outflow at the leading edge suggests the existence of a tip separation vortex which can be of small strength relative to the main vortex and which has the same direction of rotation as the main vortex. Between the main vortex and the tip separation vortex there is a region in which the induced velocities from these two vortices create a circulatory flow with rotation in the opposite direction to the other two vortices; this reversed-flow region is designated as the eddy vortex. The tip vortex causes the outflow at the leading edge, and the outflow beneath the main vortex and the inflow beneath the eddy vortex combine to form the line of ink accumulation.

From the vapor-screen photographs, a qualitative comparison can be made of the observed vortex-core positions with those calculated in reference 2. In general, the observed vortex cores are at comparable distances above the wing surface but are considerably more inboard than the calculated positions of reference 2. It can be seen from these results that theoretical calculations using a single, separated vortex pair can be applied at supersonic speeds for very slender wings.

Wings With Semiapex Angles of 15° and 22.5°

In some of the vapor-screen photographs of the wing with a semiapex angle of 15° (fig. 7), two regions of vorticity can be identified. The ink-flow photographs (fig. 19) show two lines of ink accumulation which correspond to these two regions of vorticity. The suggested explanation for these two lines of ink accumulation is similar to that given for the single line and is illustrated in the accompanying sketch.

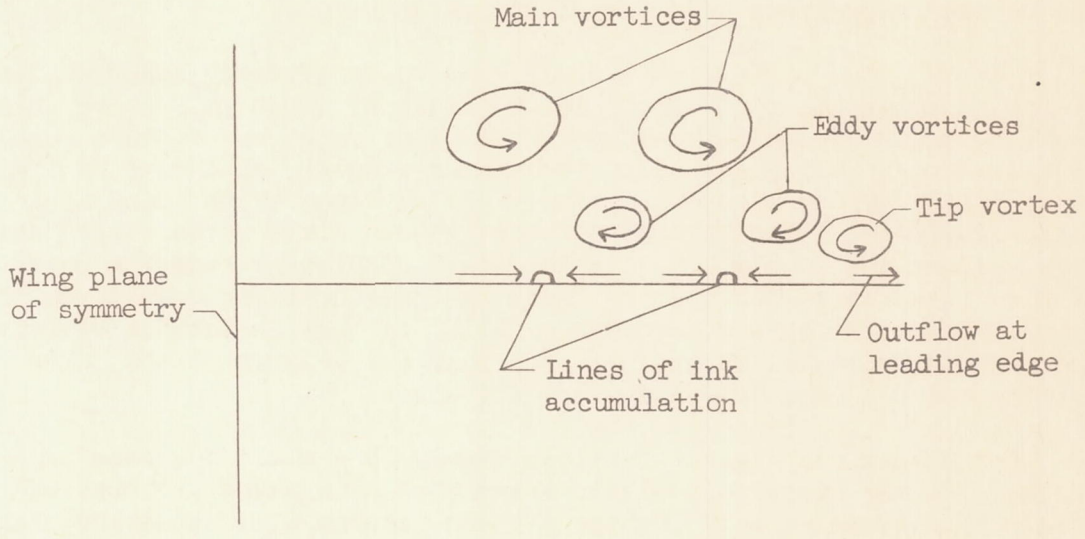

For the wing with a semiapex angle of 22.5° (fig. 8), the separated region is spread out over the outer part of the wing semispan and remains considerably closer to the wing upper surface than that for previous wings. At some angles of attack (α = 12° to 16°), there are indications of the presence of some type of disturbance, possibly a weak shock formation, but this is not distinct enough to be definitely recognizable. The ink-flow photographs in figure 20 show the same general type of flow, with one line of ink accumulation, as the small-apex-angle wings.

The wings with semiapex angles of 15° and 22.5° (figs. 13 and 14) have negative pressure peaks which extend over a large portion of the outboard region of the wings at the higher angles of attack. The abrupt spanwise decreases in pressure for some angles of attack (α = 8° to 14° in fig. 13 and α = 8° to 16° in fig. 14) correspond to the observed inboard limit of the separated region adjacent to the wing. More gradual spanwise decreases in pressure occur at the higher angles of attack where the most inboard portion of the separated region lies somewhat above the wing surface.

Wing With a Semiapex Angle of 31.75°

Shock waves are recognizable on the wing with a semiapex angle of 31.75° (fig. 9) even at small angles of attack. The shock wave moves inboard with increasing angle of attack. Between $\alpha = 14^\circ$ and 16°, a change in the appearance of the flow phenomena occurs. The changed appearance is attributed to the fact that the flat region of separated vorticity adjacent to the surface of the wing moves inboard at a faster rate than the shock wave; therefore, at angles of attack of 16° and greater, the shock wave intersects the region of vorticity and produces the unusual appearance seen in the photographs.

The ink-flow pictures (fig. 21) show the previously observed line of ink accumulation up to an angle of attack of about 16°, above which the flow becomes somewhat confused. An interpretation of these results is as follows: The presence of ink at the wing tip is caused by the outward flow of ink along the blunt trailing edge. With increasing angle of attack, the bubble of ink moves forward along the wing leading edge and, at about $\alpha = 16^\circ$, ink from this bubble and from the outer orifice interferes with the ink from the other orifices. Ink from the outer orifice proceeds downstream parallel to the free-stream velocity, whereas ink from the inboard orifices passes over that of the outer orifice and proceeds toward the leading edge.

For almost all angles of attack, there is a small decrease in pressure at the spanwise position where the shock waves are observed (fig. 15). Above $\alpha = 14^\circ$, where a change in the flow appearance takes place, practically all the pressure decrease occurs at the most inboard extent of the region of separation. For these high angles of attack, the shock waves appear to intersect the relatively thick region of vorticity, and apparently the shock waves have little direct effect on the surface pressure distributions.

Comparison With Theoretical Calculations

Comparisons of pressure distributions calculated by the method of reference 2 with the measured distributions for the wing with a semiapex angle of 5° are given in figure 22. In preparing figure 22, the experimental points from figure 10 have been plotted in the positions in which they appear when the pressures for zero angle of attack are shifted to the zero-pressure-coefficient axis.

The experimental points are in general agreement with the calculated results except where the sharp negative pressure peaks occur in the calculated curves. These negative pressure peaks are the result of the assumption in the theory that the separated vorticity is concentrated in point vortex cores, which thus have a large influence on

the surface pressures beneath them. Since in the physical flow the vorticity cannot be concentrated in a point vortex and, furthermore, since all the vorticity in the physical flow is probably not in the vortex core but partly in a special vortex sheet, large negative pressure peaks are not anticipated. However, the comparisons of figure 22 show that the calculated pressure distributions of reference 2 have correct general trends in predicting large loadings over the outboard part of the span, although the calculations overestimate the negative pressure peaks. The integrated experimental pressure distributions yield results for the lift coefficients which approach the calculated results as the apex angle of the wing is reduced, as shown previously from force tests in reference 2.

CONCLUDING REMARKS

The results of the present tests indicated that separated regions of vorticity existed along the chords of all the wings in the series tested. Concentrated vortex cores were found only on wings with semiapex angles of 5°, 7.5°, and 10°. For wings with semiapex angles of 15°, 22.5°, and 31.75°, the separated vorticity was concentrated in a region extending over the outboard part of the span and lying close to the wing upper surface.

The results show that aerodynamic calculations, such as those in NACA TN 3430, utilizing a single, separated vortex pair above the wing upper surface to represent the separated vorticity can be applied at supersonic speeds for very slender wings. From a qualitative standpoint, the observed vortex cores on these very slender wings were located at distances above the wing surfaces comparable with the calculated positions but considerably more inboard than the calculated positions. The physical nature of the separation phenomena presented for the wings with the higher apex angles could be a guide for additional analyses.

Langley Aeronautical Laboratory,
National Advisory Committee for Aeronautics,
Langley Field, Va., May 12, 1955.

APPENDIX

DISCUSSION OF VAPOR-SCREEN OBSERVATIONS

In order to evaluate the vapor-screen photographs, the nature of the observed flow must be understood. As has been mentioned previously, the water is broken up by the turbulence screens and appears in the test section as a fog. These particles are sufficiently small so that they follow the streamlines of the air flow, and, by observing the illuminated particles, certain characteristics of the flow can be deduced.

The regions of contrasting illumination which show up in the photographs are, of course, the results of variations in the concentration per unit volume of the particles in the region illuminated by the slit of light. Regions containing large numbers of particles per unit volume scatter a large amount of light and appear as light regions and conversely for regions containing small numbers of particles. The very bright straight line which appears in each photograph is simply the reflection of the narrow slit of light from the wing surface and serves to define the span of the wing at the chord station being considered.

From overall observation of the photographs, some reasonable identifications can be given to certain areas. One or more dark regions are seen in most of the vapor-screen photographs. These dark regions are identified as follows: isolated circular regions which are undoubtedly vortex cores, regions of separation which undoubtedly contain vorticity and are located near the upper surfaces of the wings, regions outside the Mach cone, and regions outboard of the shock waves on the wings. All of these can be shown to be regions in which the density of the air is less than that in adjacent regions. It would thus appear that the concentration of particles in a given region and, therefore, the illumination of the region are approximately proportional to the density of the air in that region.

Additional factors which might be expected to affect the illumination to a certain degree are temperature changes and centrifugal-force effects. Large temperature changes which might vaporize or condense particles in certain regions could possibly have some effects on the illumination. However, when the time intervals involved in the passage of particles along the chord of the wings are considered, it is doubtful that there can be sufficient transfer of heat to affect appreciably the particle concentration through vaporization or condensation.

In addition to the dark regions in the vapor-screen photographs, there are also some very light regions, or regions of high density, which originate at the leading edges of the wings with the smallest

apex angles. These high-density regions are the result of particles "piling up" on the lower surface of the wing and leaving the lower surface at the wing leading edge. The particles are influenced by complex forces, which include centrifugal forces, in the region above the wing surface. The centrifugal forces probably cause the light regions inboard of the vortex cores on some of the wings with the small apex angles. As the apex angle of the wing is increased, the velocity normal to the leading edge is increased and fewer particles leave the wing; thus the intensity of the illumination near the leading edge is decreased.

REFERENCES

1. Spreiter, John R., and Sacks, Alvin H.: The Rolling Up of the Trailing Vortex Sheet and Its Effect on the Downwash Behind Wings. Jour. Aero. Sci., vol. 18, no. 1, Jan. 1951, pp. 21-32, 72.

2. Brown, Clinton E., and Michael, William H., Jr.: On Slender Delta Wings With Leading-Edge Separation. NACA TN 3430, 1955.

3. Allen, H. Julian, and Perkins, Edward W.: A Study of Effects of Viscosity on Flow Over Slender Inclined Bodies of Revolution. NACA Rep. 1048, 1951. (Supersedes NACA TN 2044.)

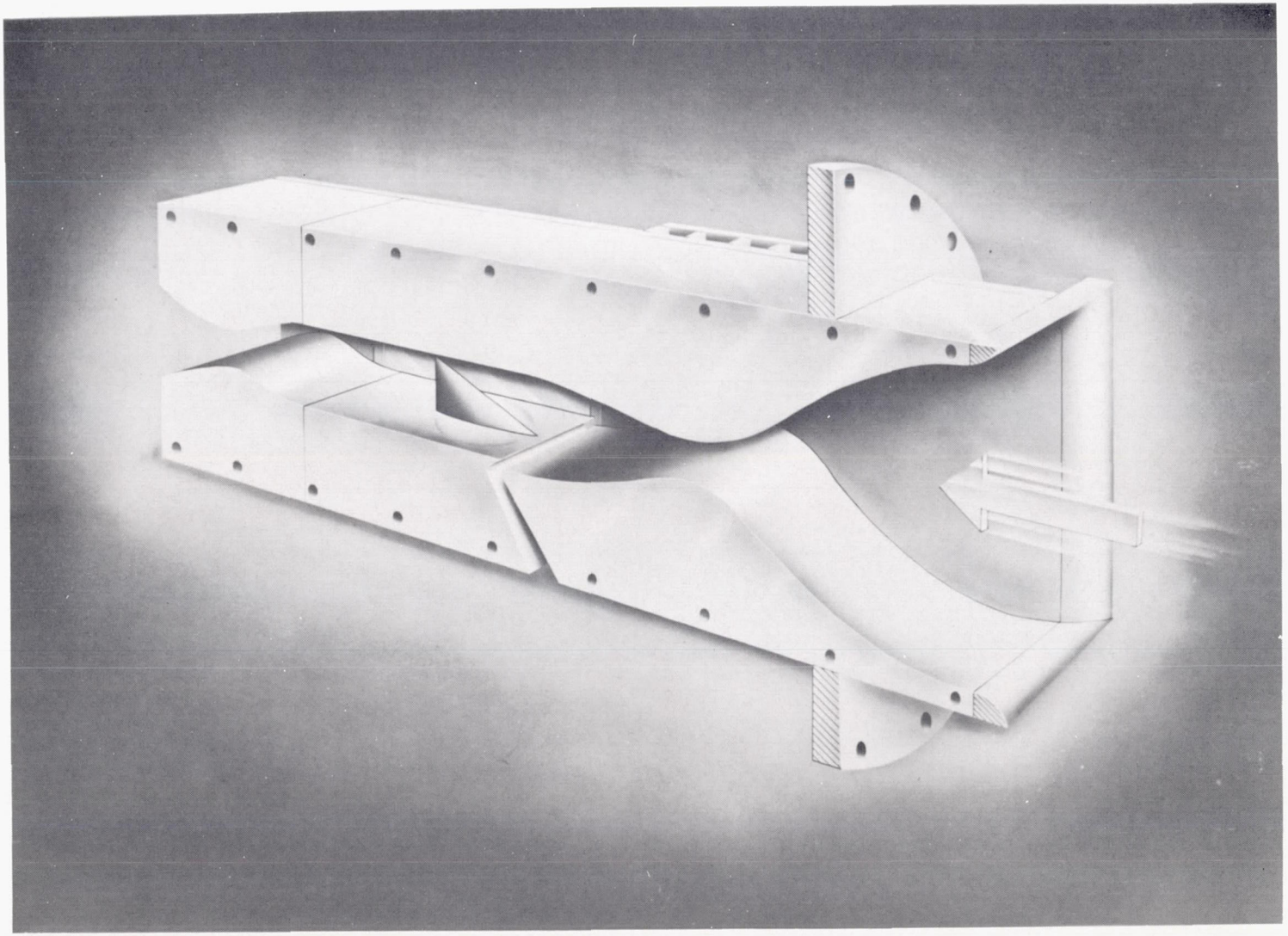

L-80472

Figure 1.- View of blowdown jet showing the boundary-layer removal scoop.

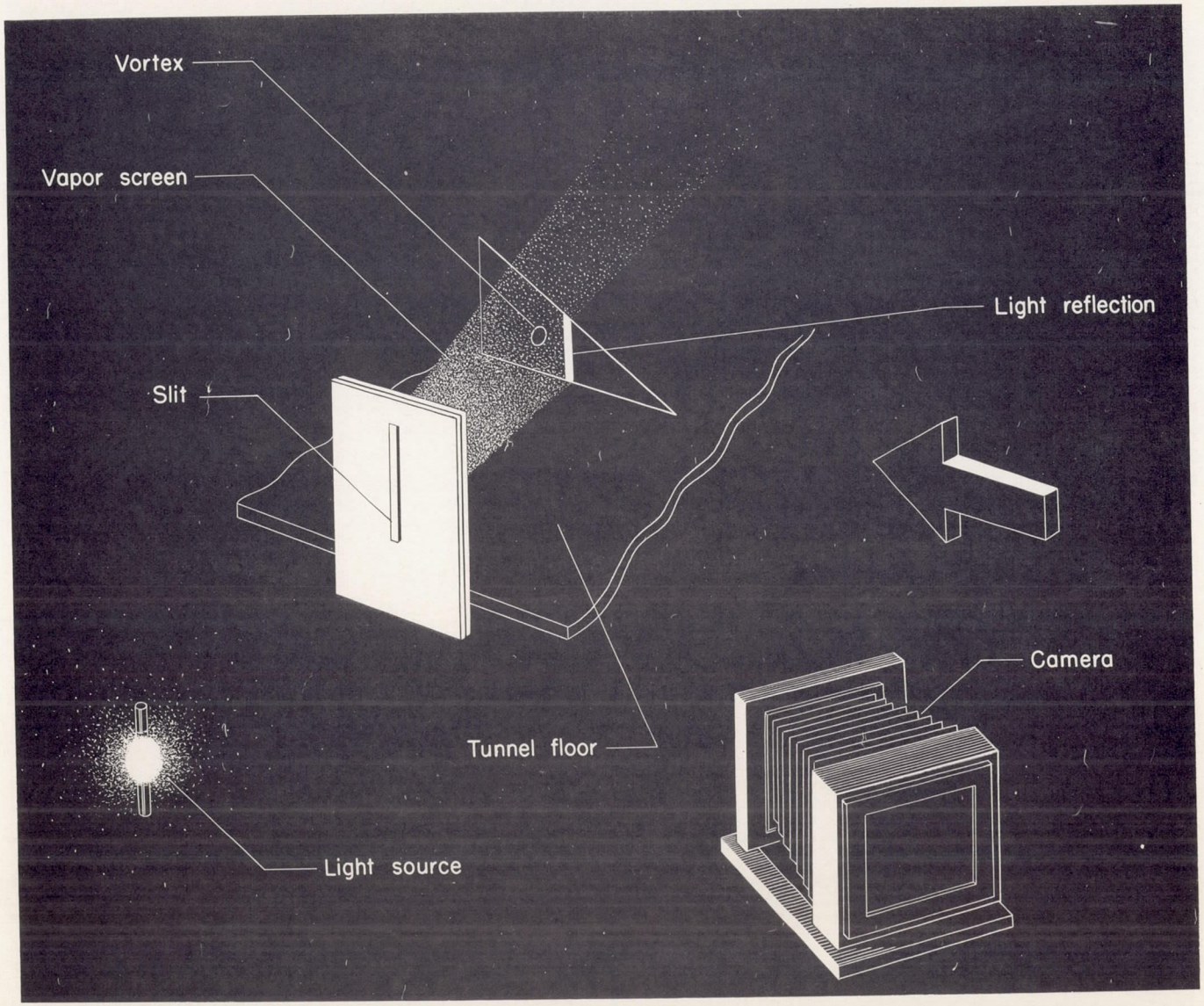

Figure 2.- Schematic drawing of vapor-screen apparatus and setup.

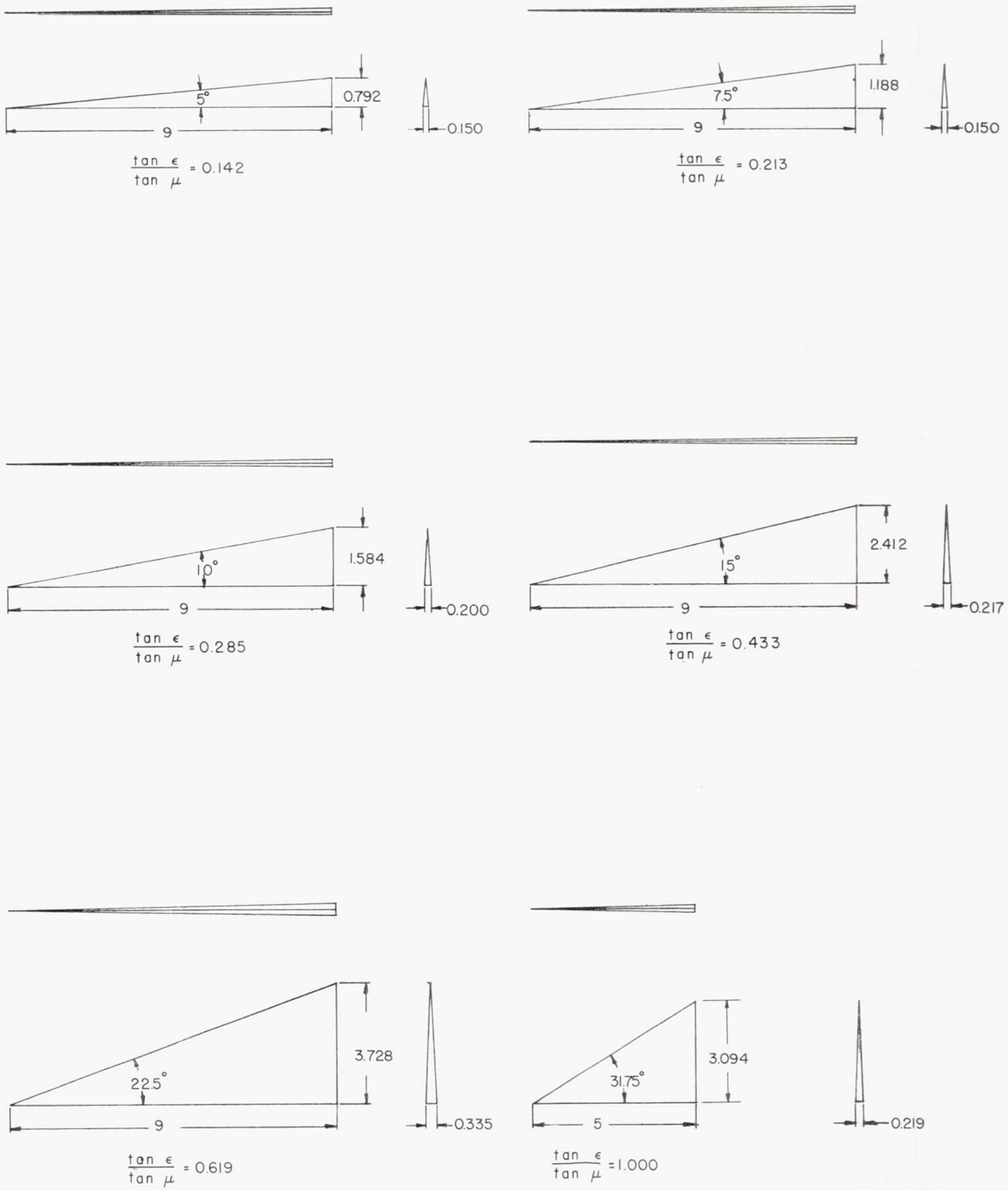

Figure 3.- Drawings of models used in this investigation. All dimensions are in inches.

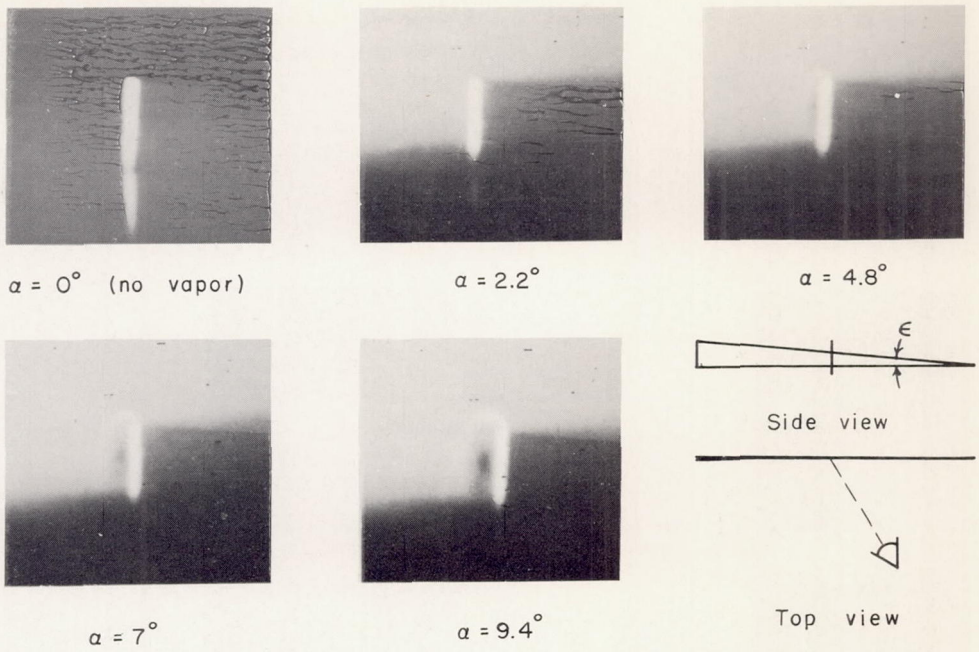

(a) 51.4-percent-chord position.

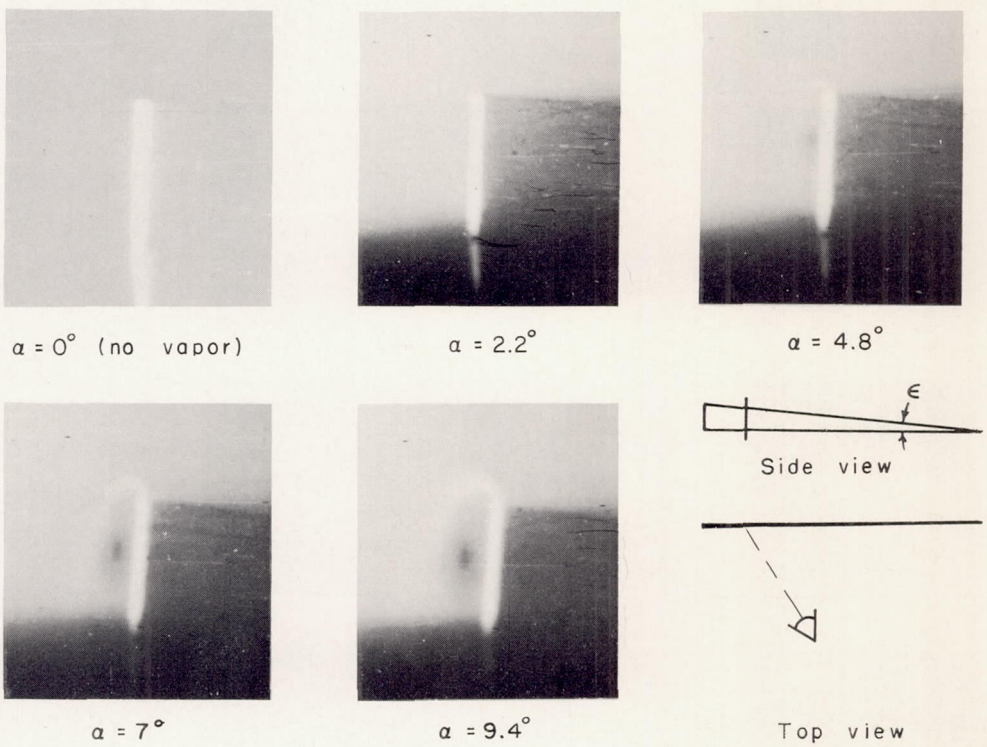

(b) 84.7-percent-chord position.

L-87982

Figure 4.- Vapor-screen photographs of the flow over wing with semiapex angle of 5°.

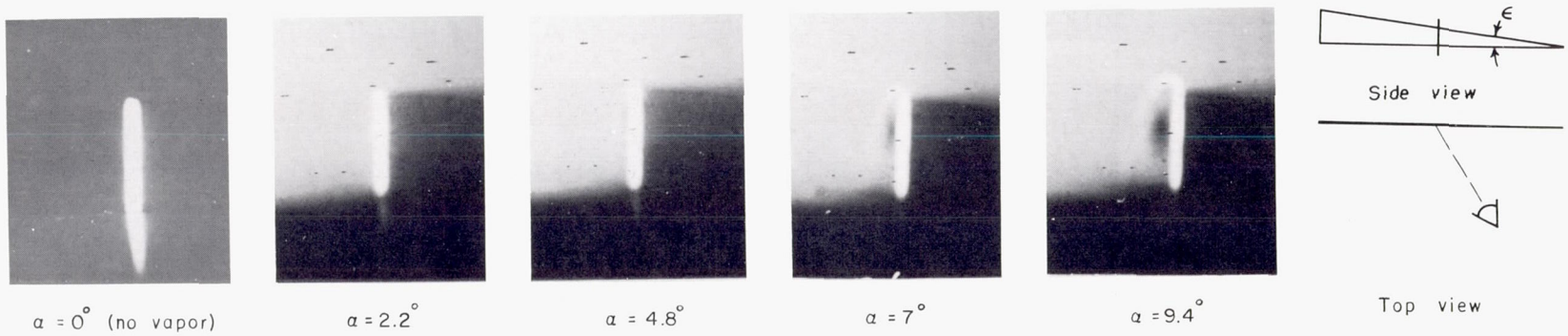

(a) 51.4-percent-chord position.

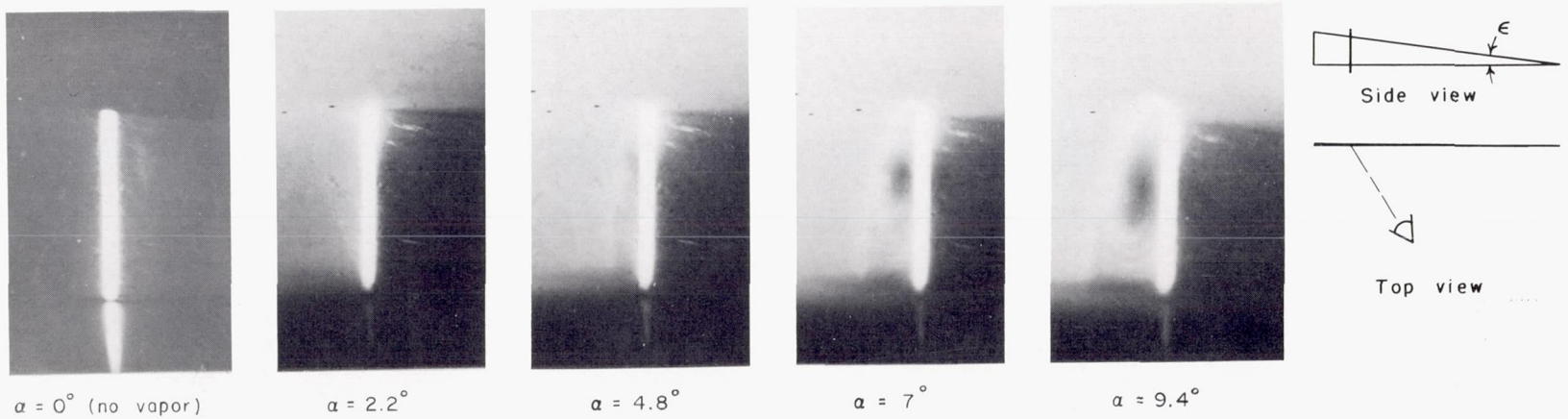

L-87983

(b) 84.7-percent-chord position.

Figure 5.- Vapor-screen photographs of the flow over wing with semiapex angle of 7.5°.

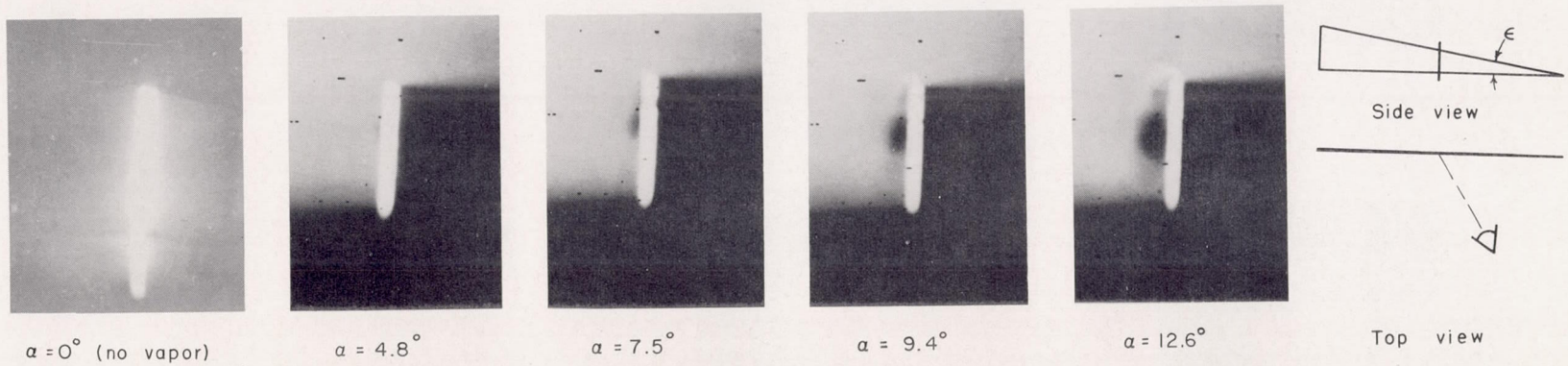

(a) 51.4-percent-chord position.

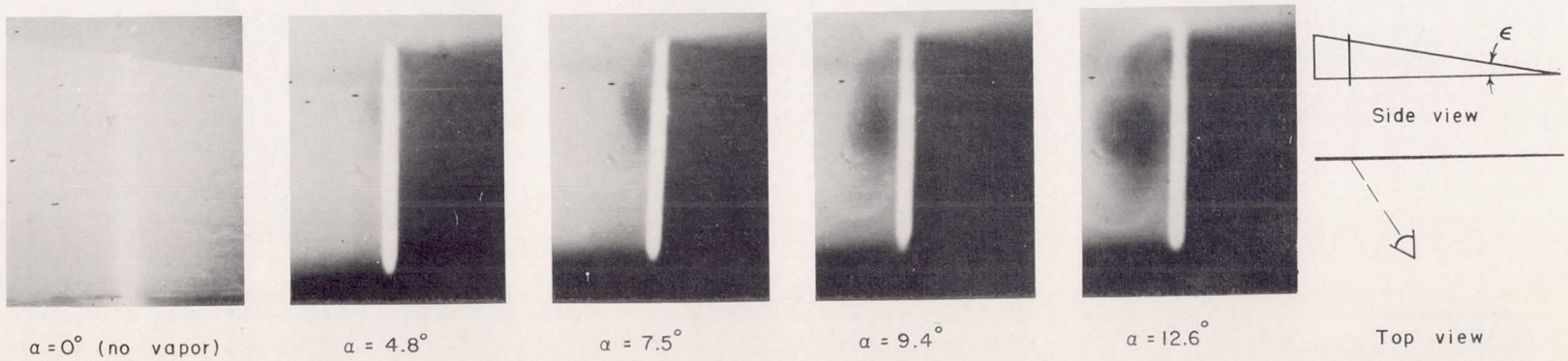

(b) 84.7-percent-chord position.

L-87984

Figure 6.- Vapor-screen photographs of the flow over wing with semiapex angle of 10°.

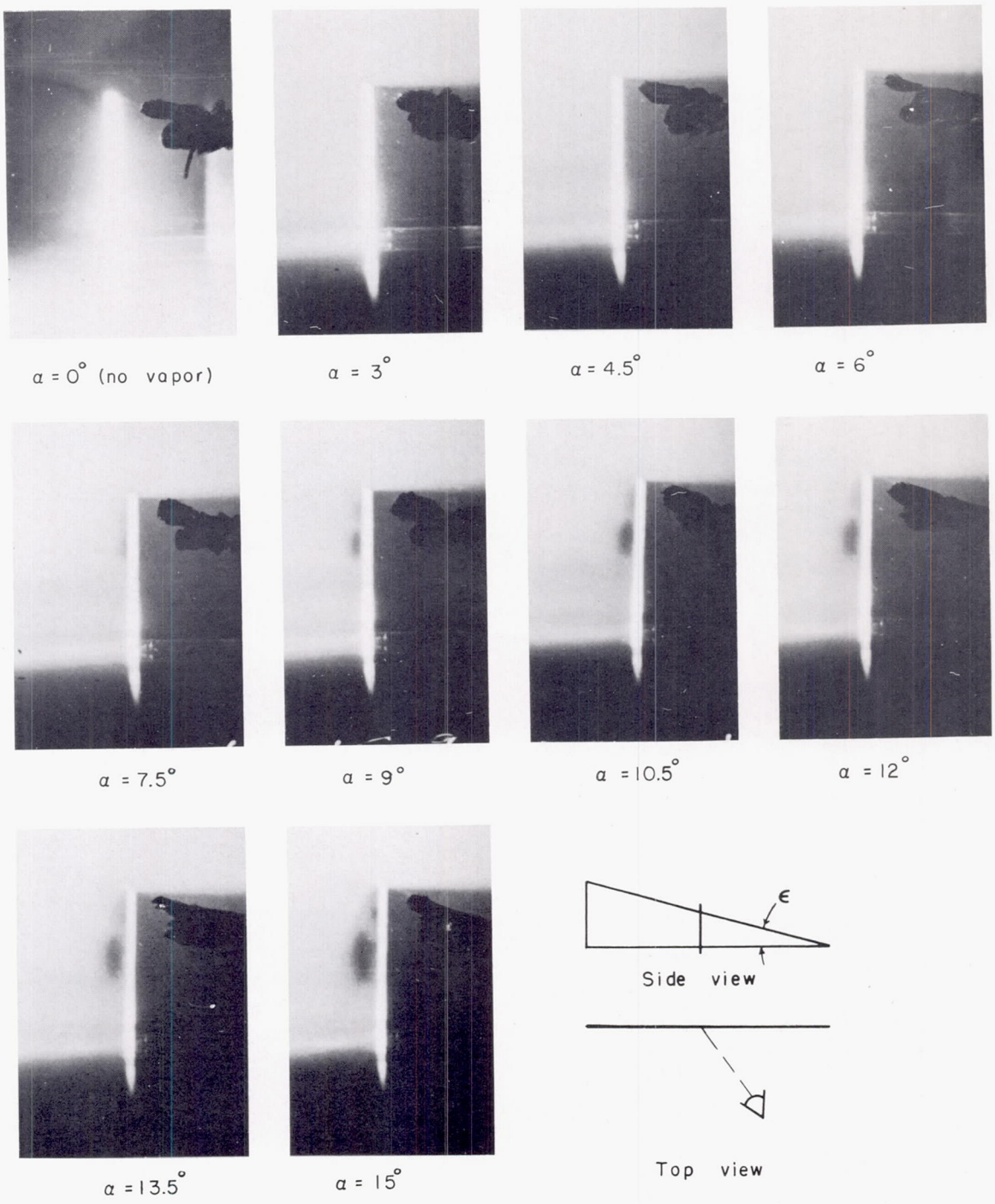

(a) 52.8-percent-chord position. L-87985

Figure 7.- Vapor-screen photographs of the flow over wing with semiapex angle of 15°.

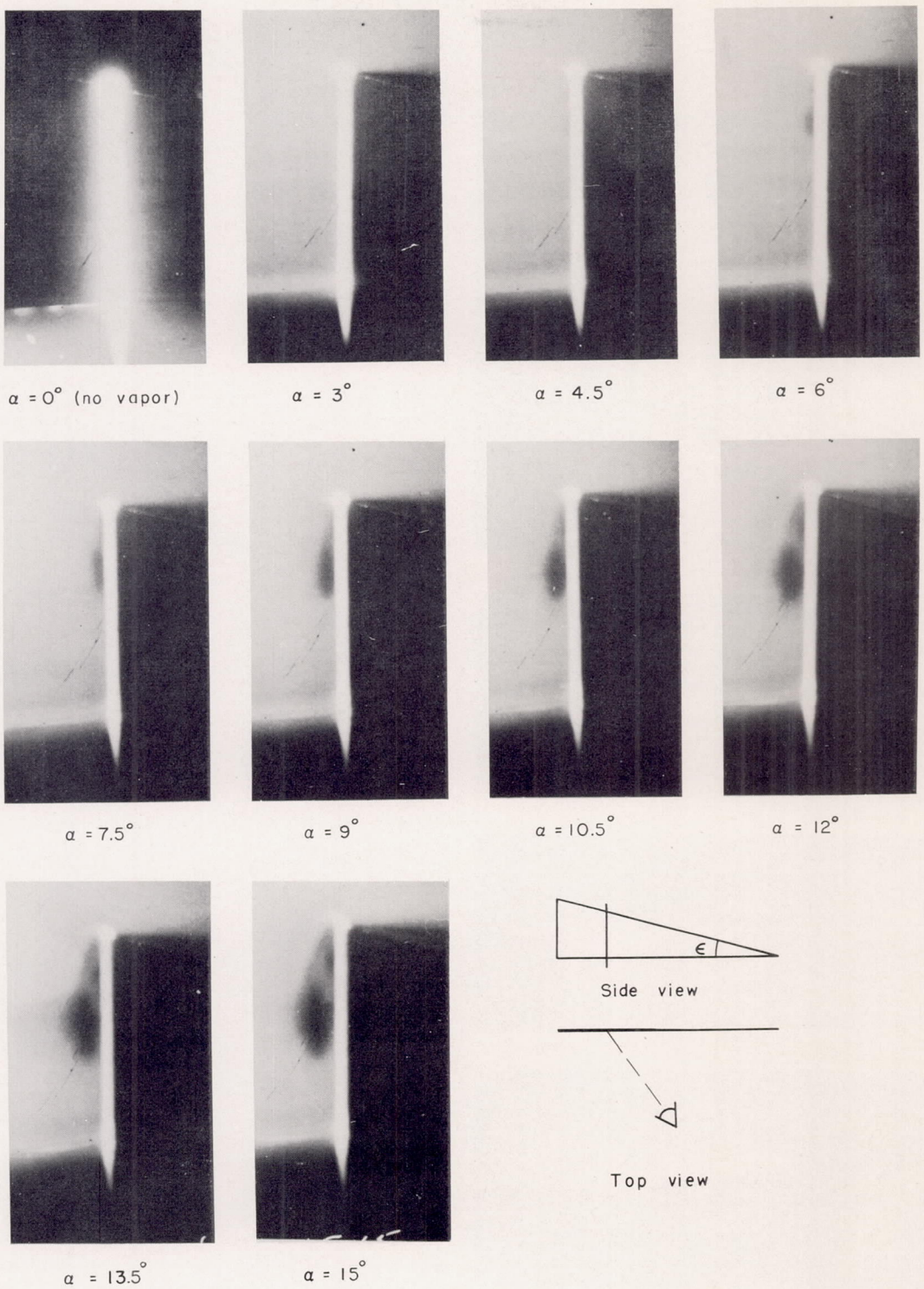

(b) 77.9-percent-chord position. L-87986

Figure 7.- Concluded.

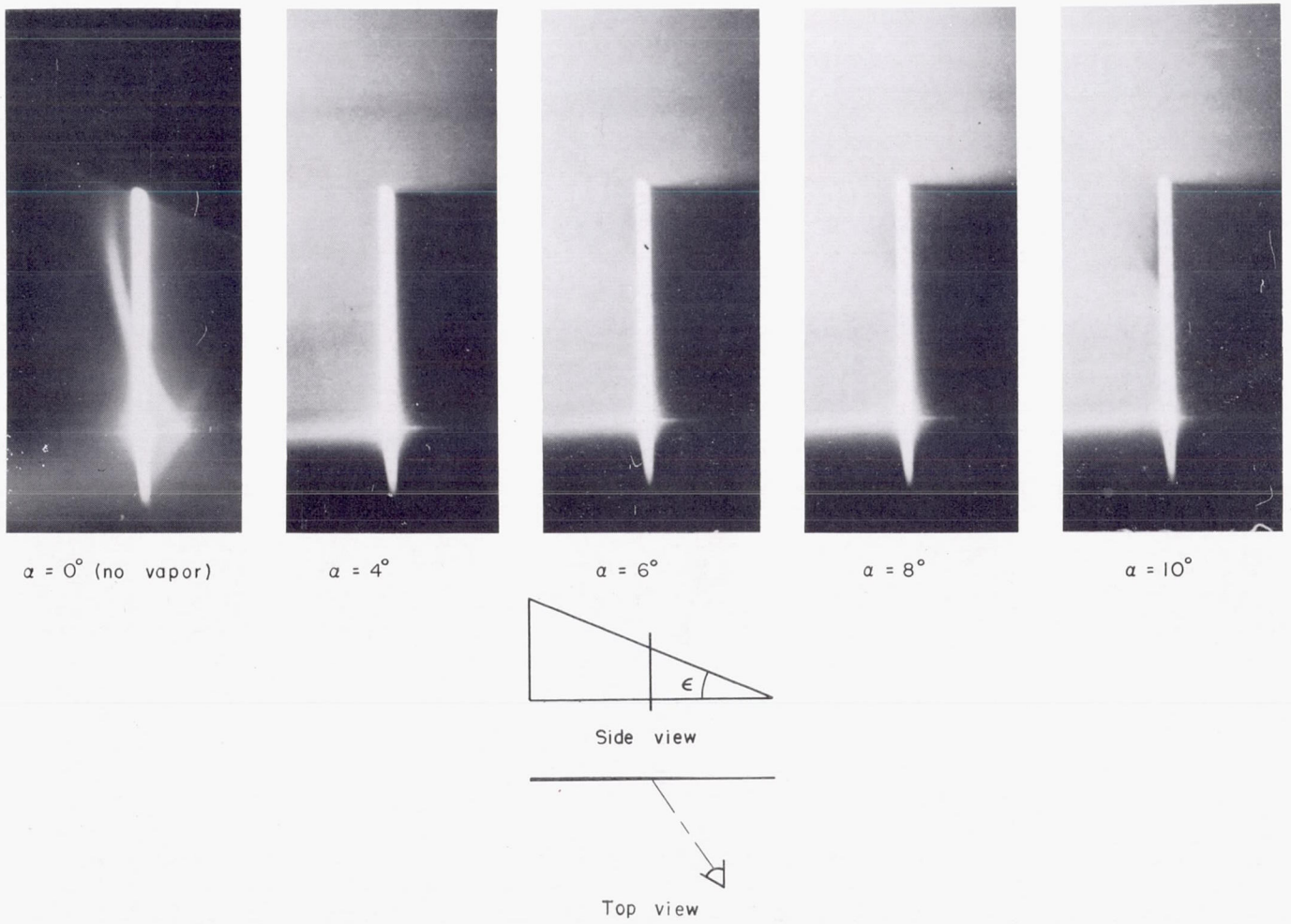

(a) 50.0-percent-chord position. L-87987

Figure 8.- Vapor-screen photographs of the flow over wing with semiapex angle of 22.5°.

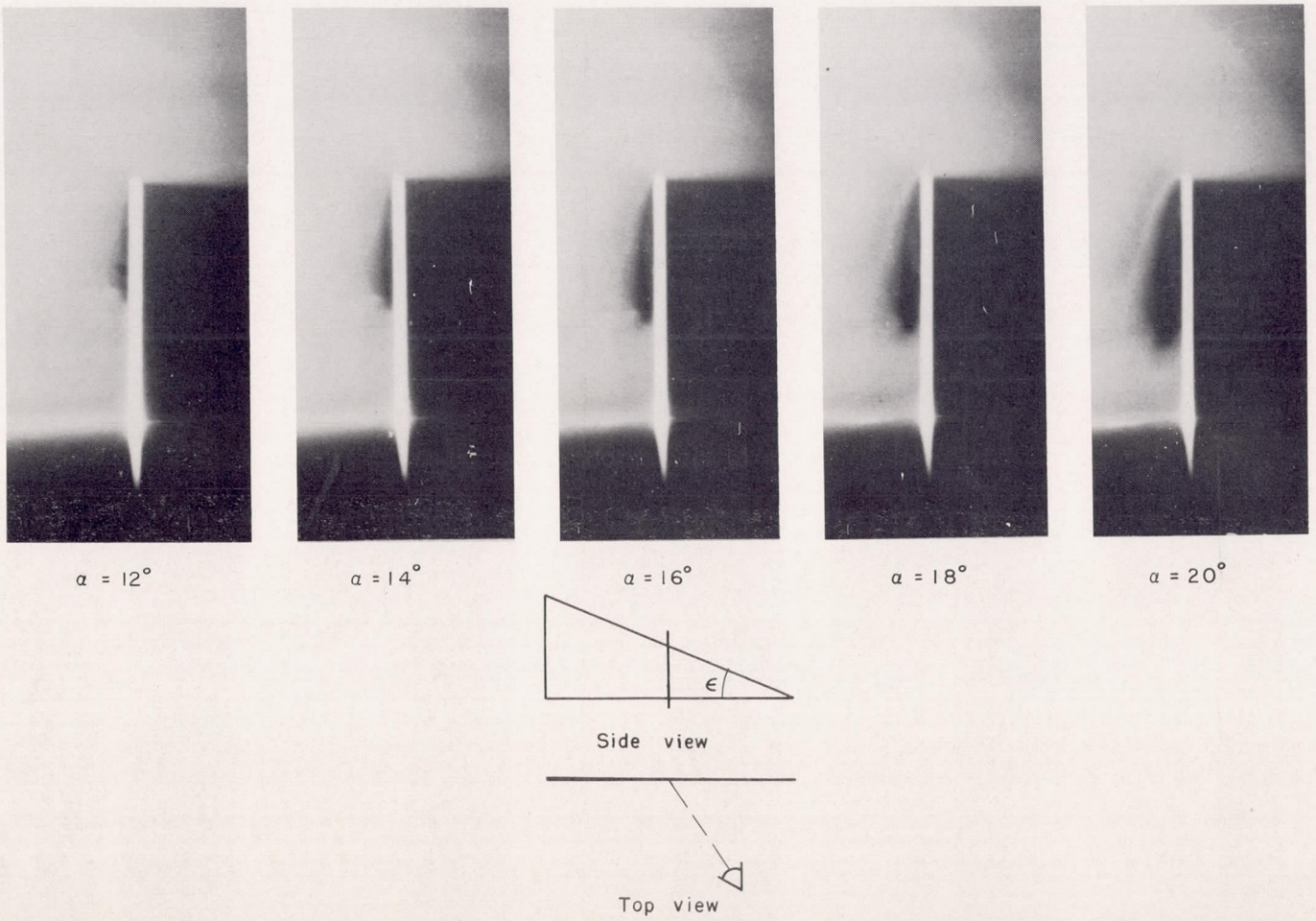

(a) Concluded.

L-87988

Figure 8.- Continued.

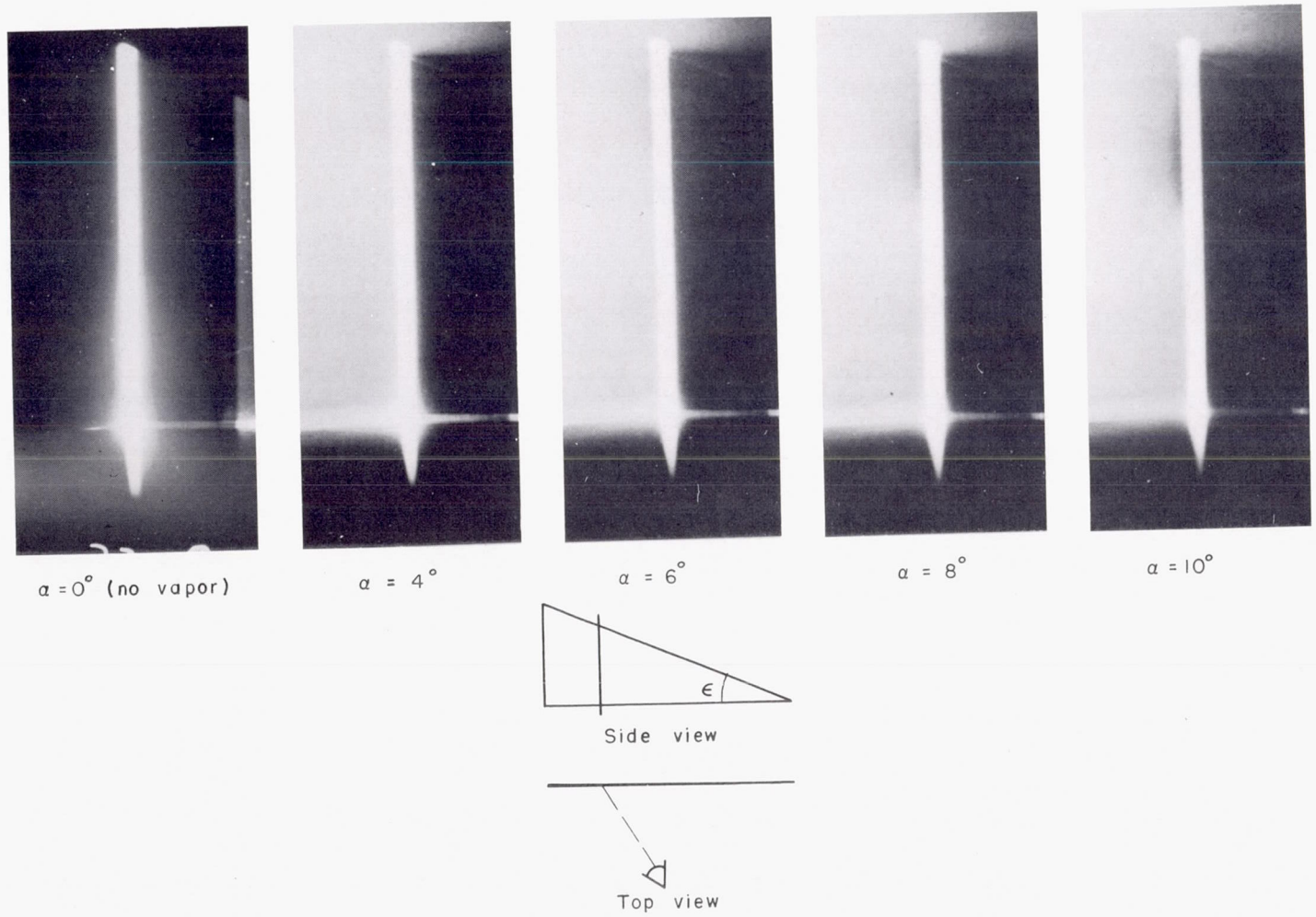

L-87989

(b) 77.9-percent-chord position.

Figure 8.- Continued.

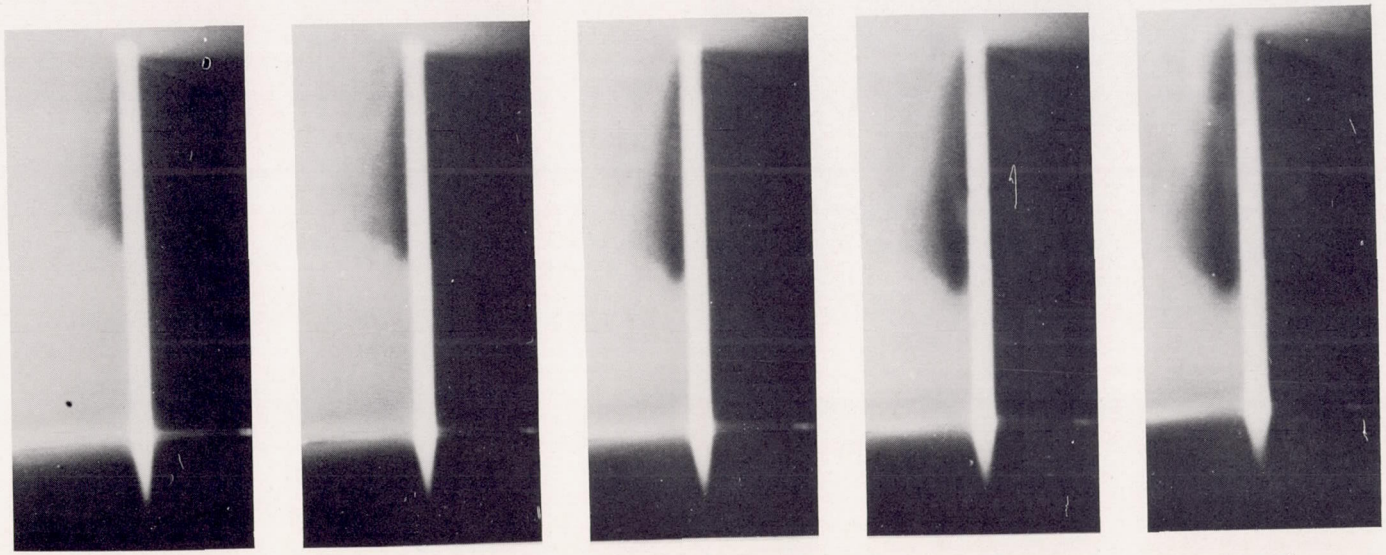

L-87990

(b) Concluded.

Figure 8.- Concluded.

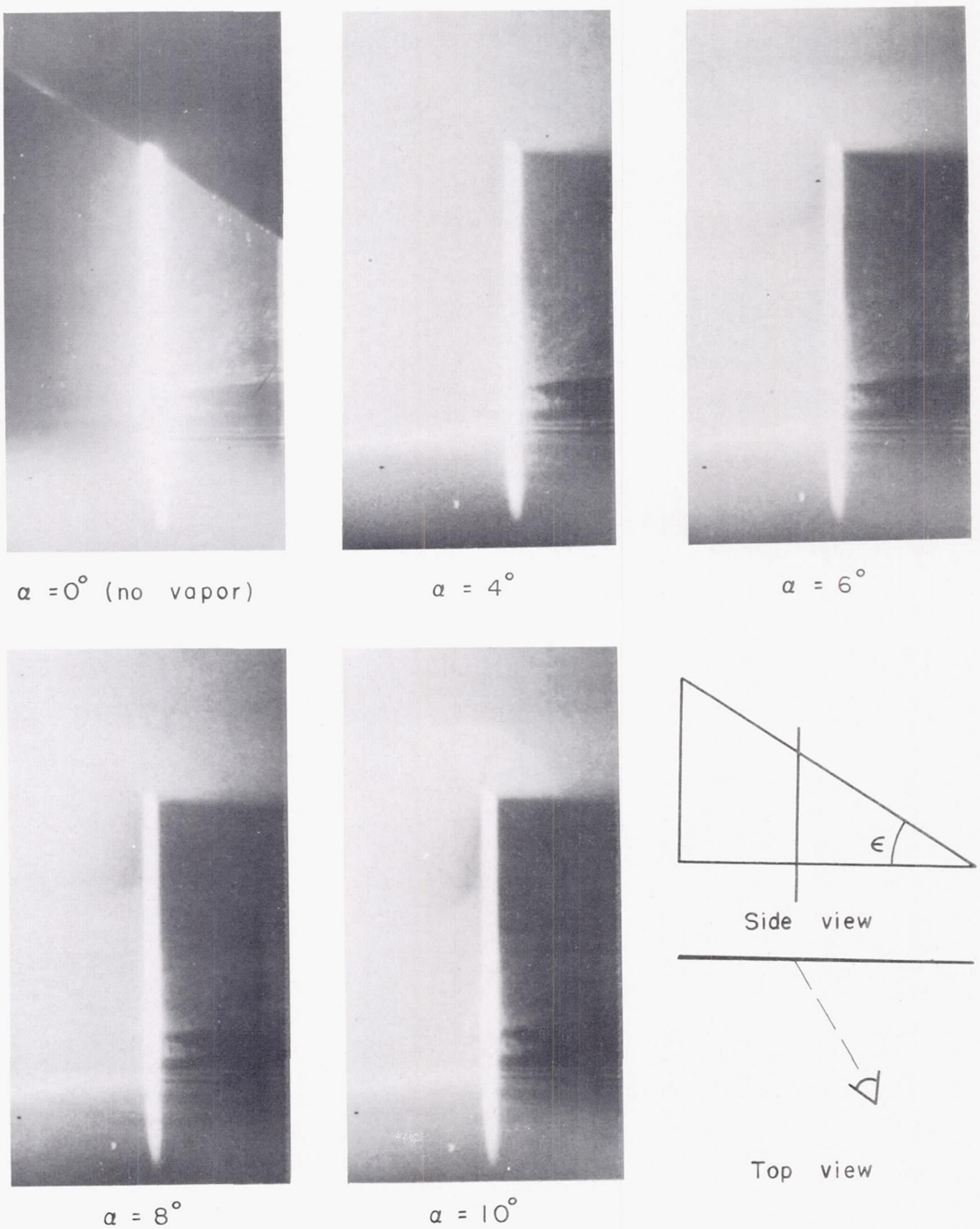

(a) 60.0-percent-chord position. L-89292

Figure 9.- Vapor-screen photographs of the flow over wing with semiapex angle of 31.75°.

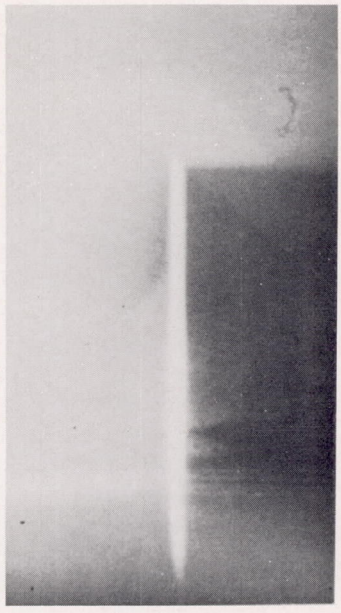

$\alpha = 12°$

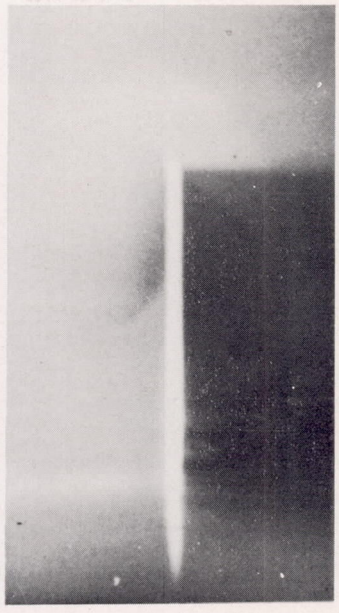

$\alpha = 14°$

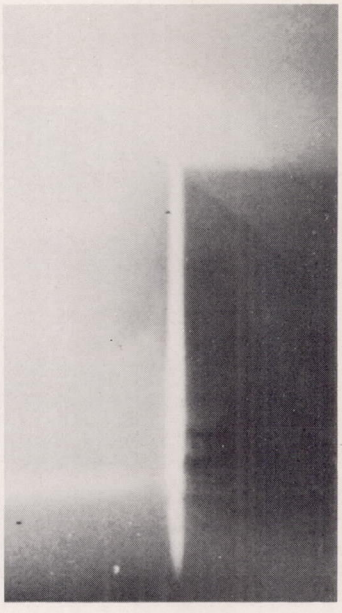

$\alpha = 16°$

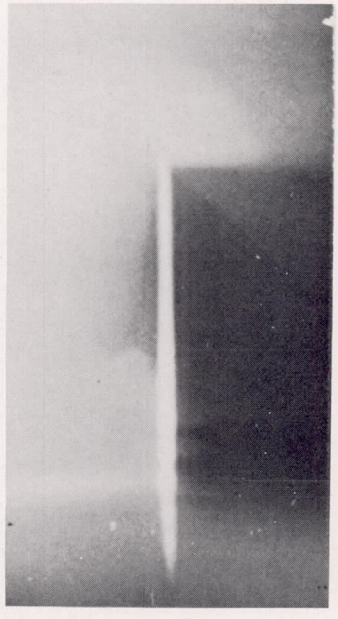

$\alpha = 18°$

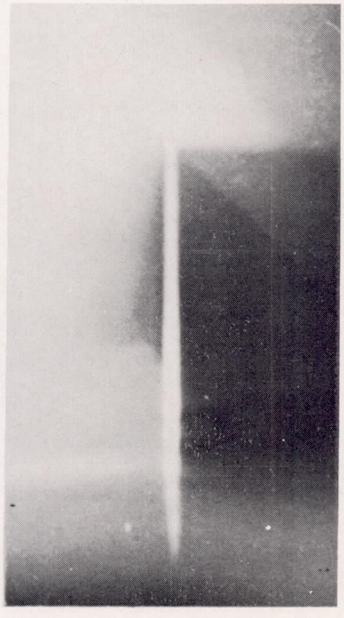

$\alpha = 20°$

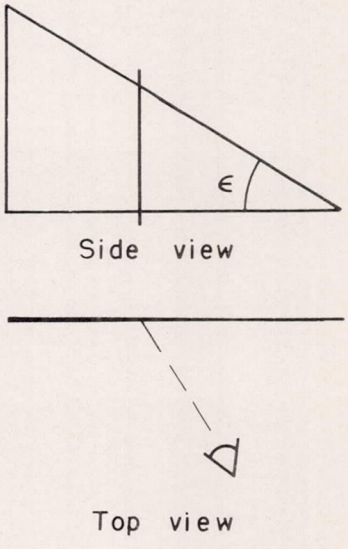

L-89293

(a) Concluded.

Figure 9.- Continued.

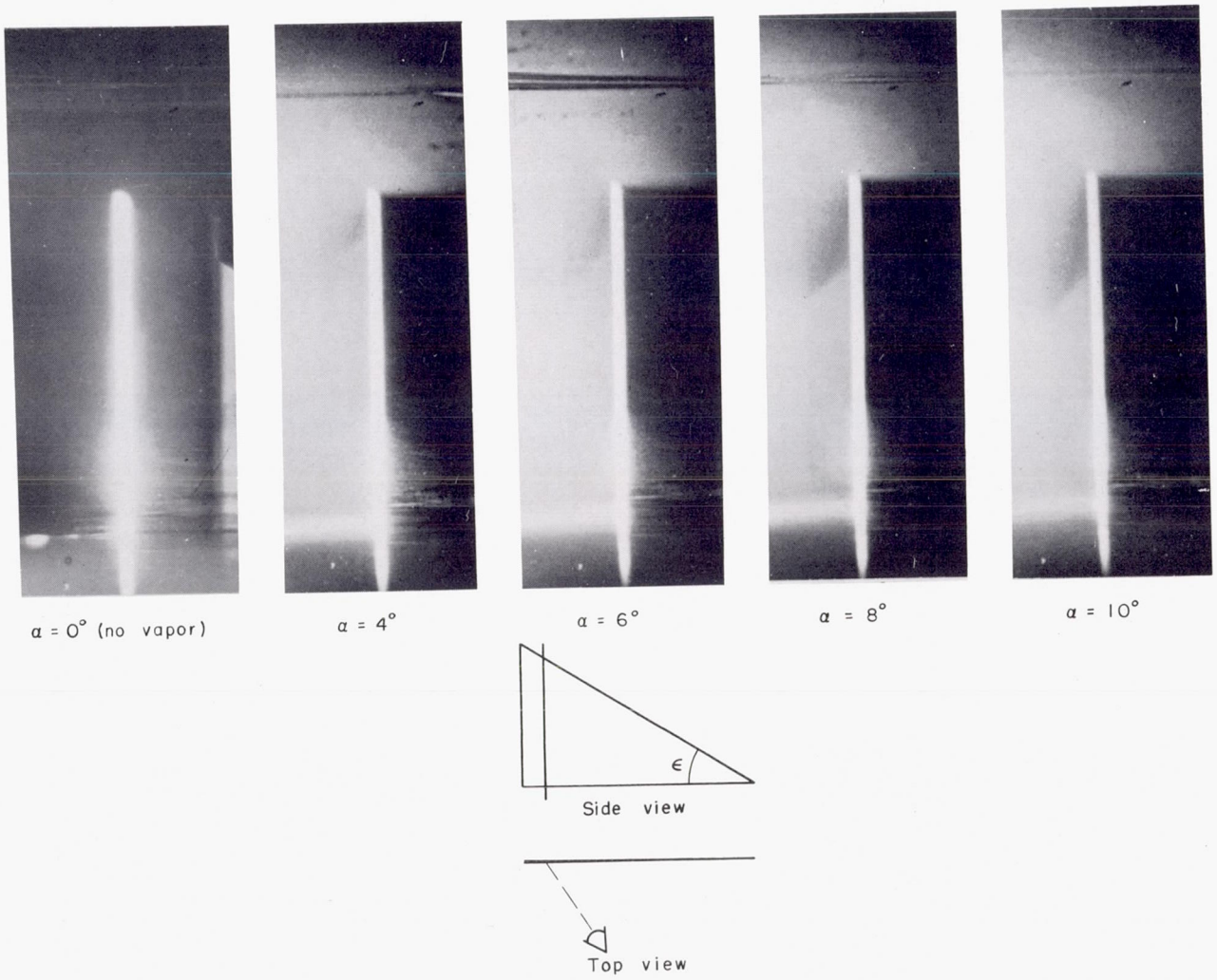

L-89294

(b) 90.0-percent-chord position.

Figure 9.- Continued.

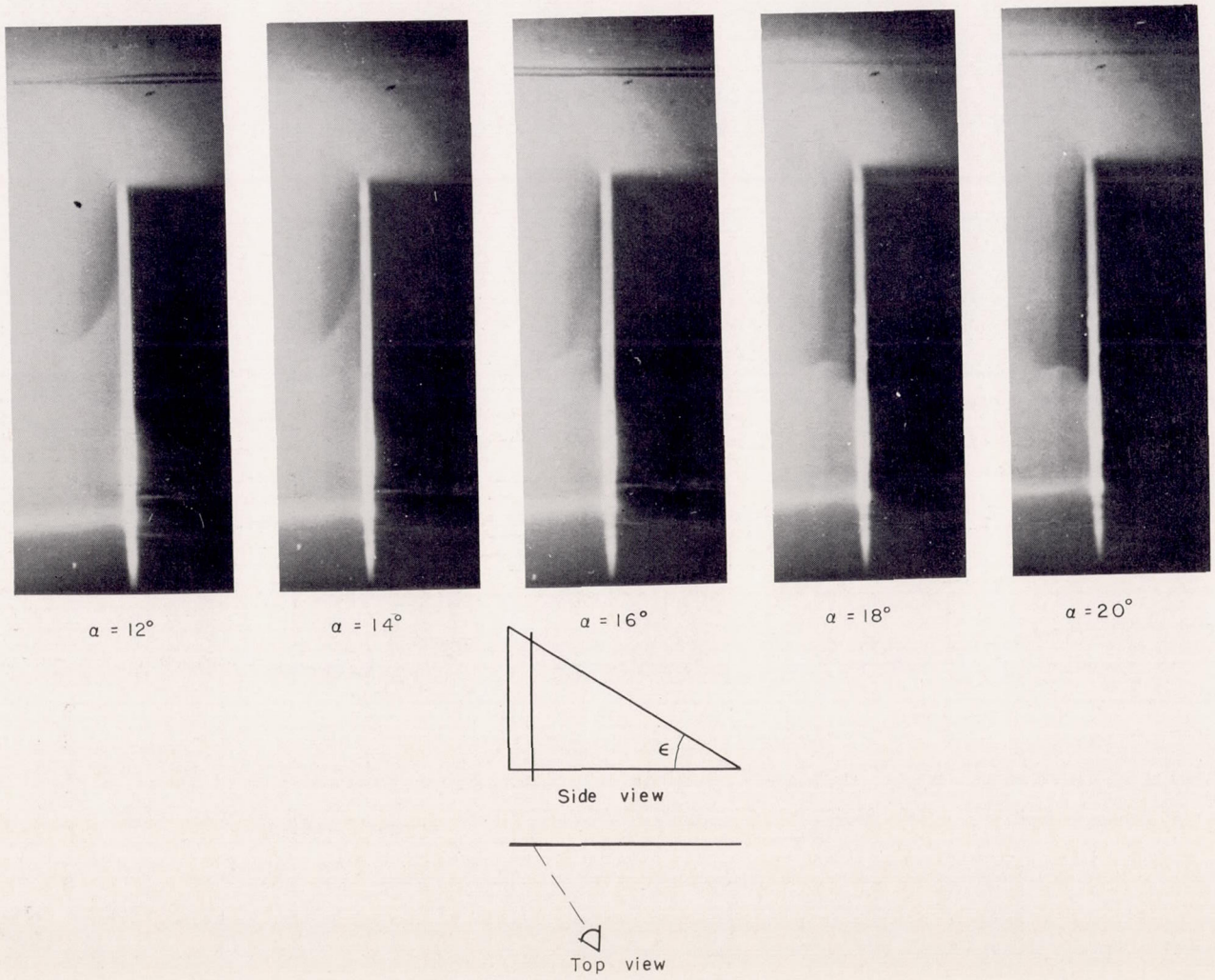

L-89295

(b) Concluded.

Figure 9.- Concluded.

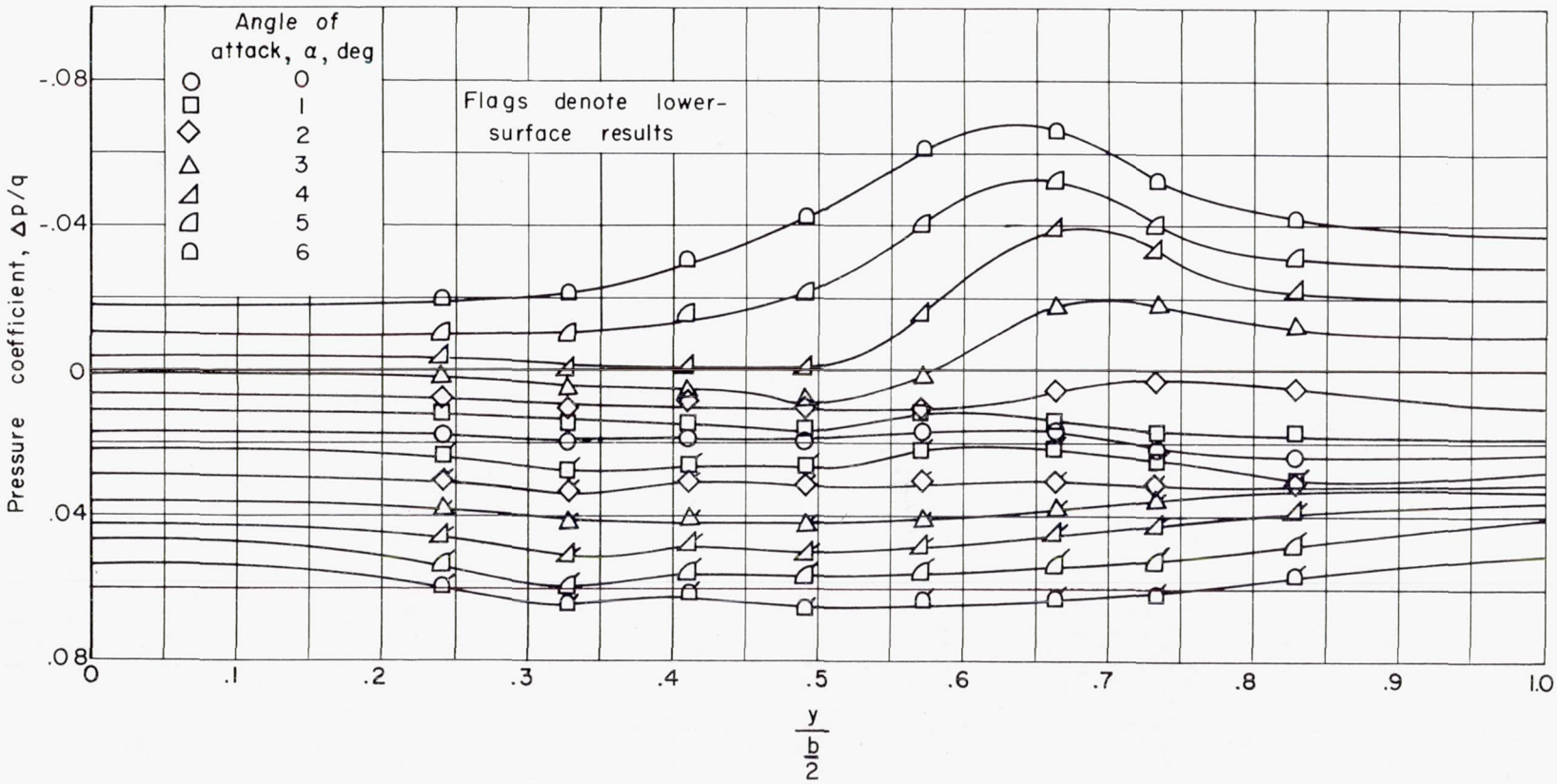

Figure 10.- Spanwise pressure distribution on wing with semiapex angle of 5°. Orifices located at 78-percent-chord position.

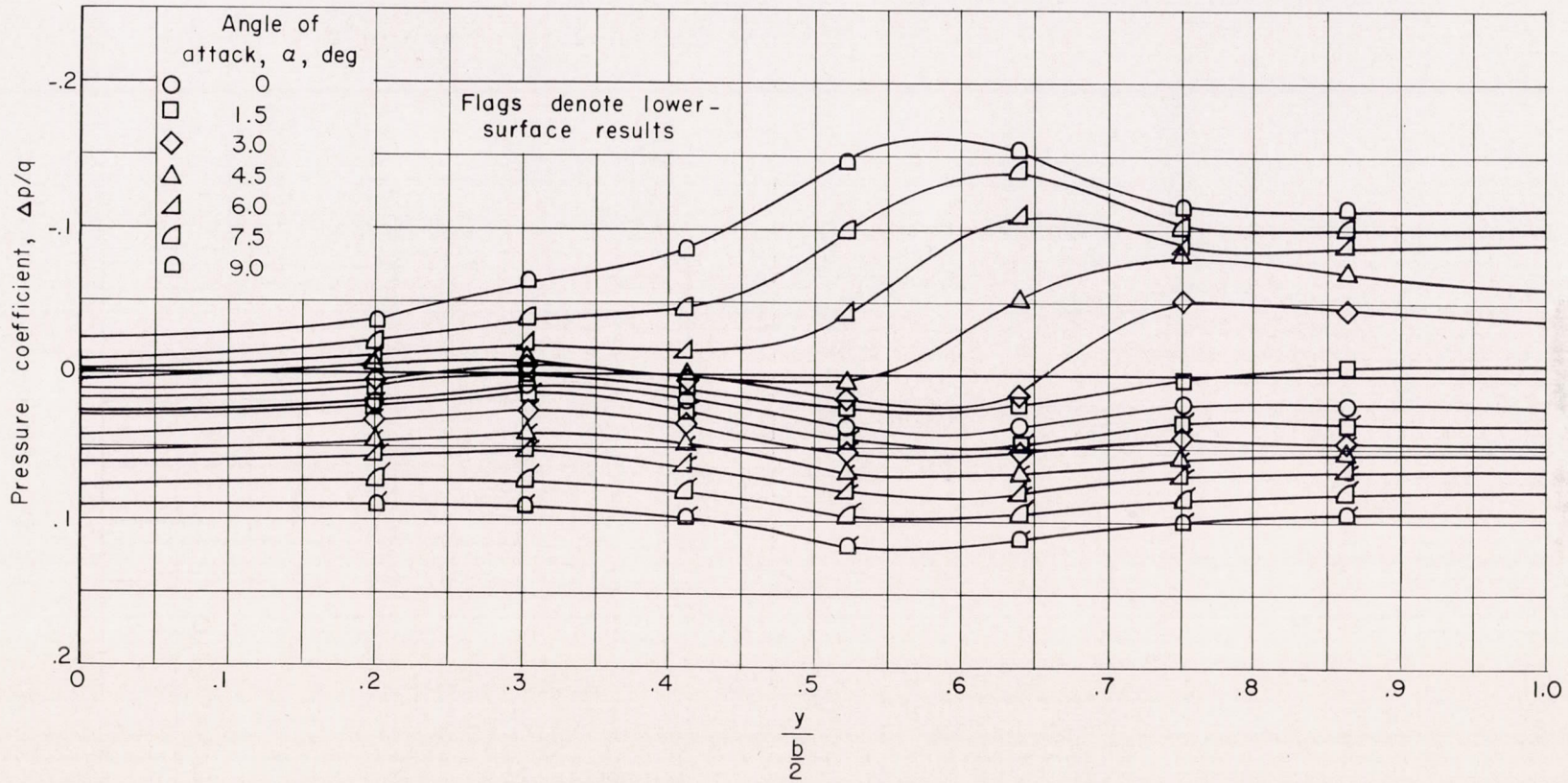

Figure 11.- Spanwise pressure distributions on wing with semiapex angle of 7.5°. Orifices located at 56-percent-chord position.

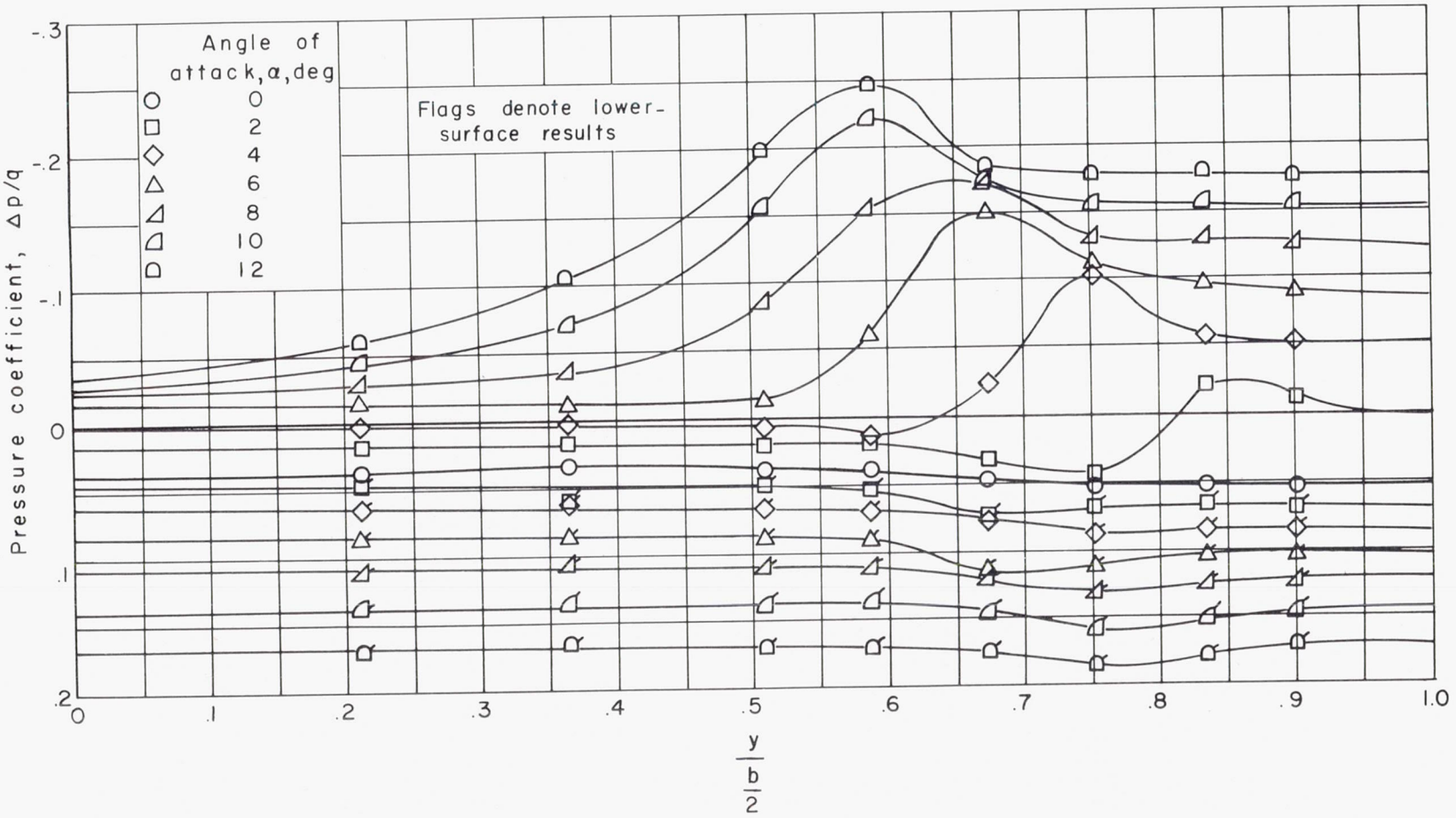

Figure 12.- Spanwise pressure distributions on wing with semiapex angle of 10°. Orifices located at 50-percent-chord position.

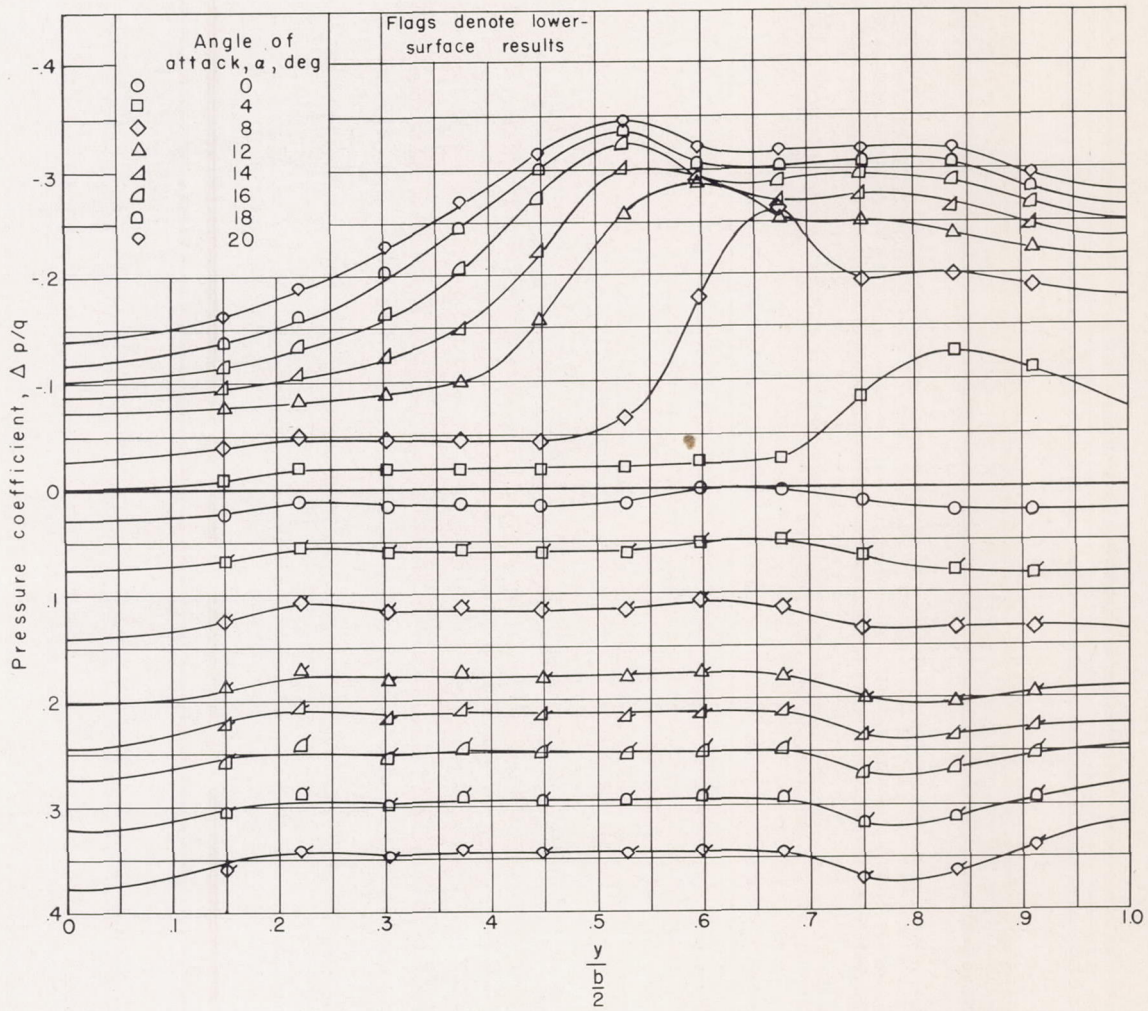

Figure 13.- Spanwise pressure distributions on wing with semiapex angle of 15°. Orifices located at 56-percent-chord position.

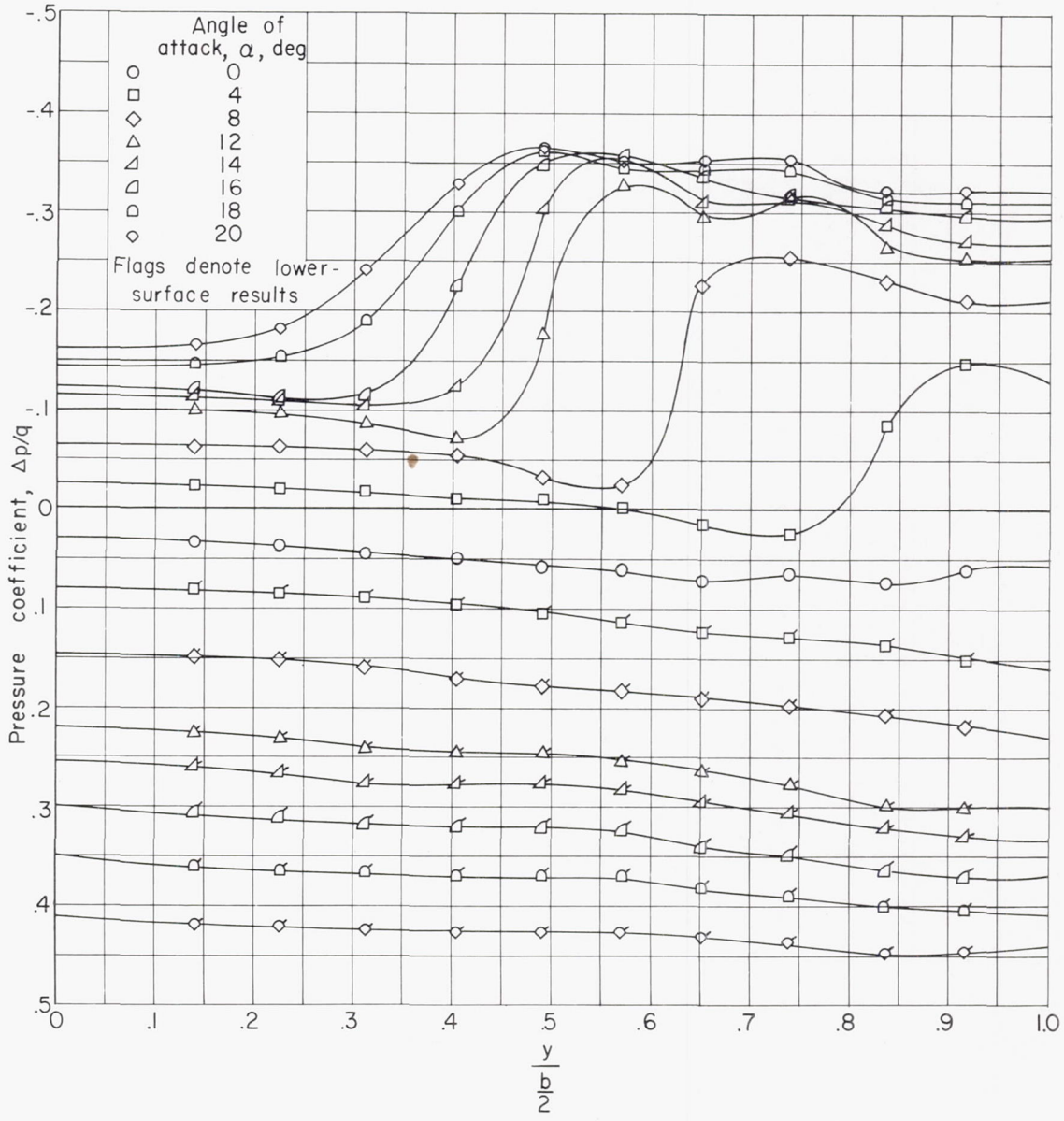

Figure 14.- Spanwise pressure distributions on wing with semiapex angle of 22.5°. Orifices located at 39-percent-chord position.

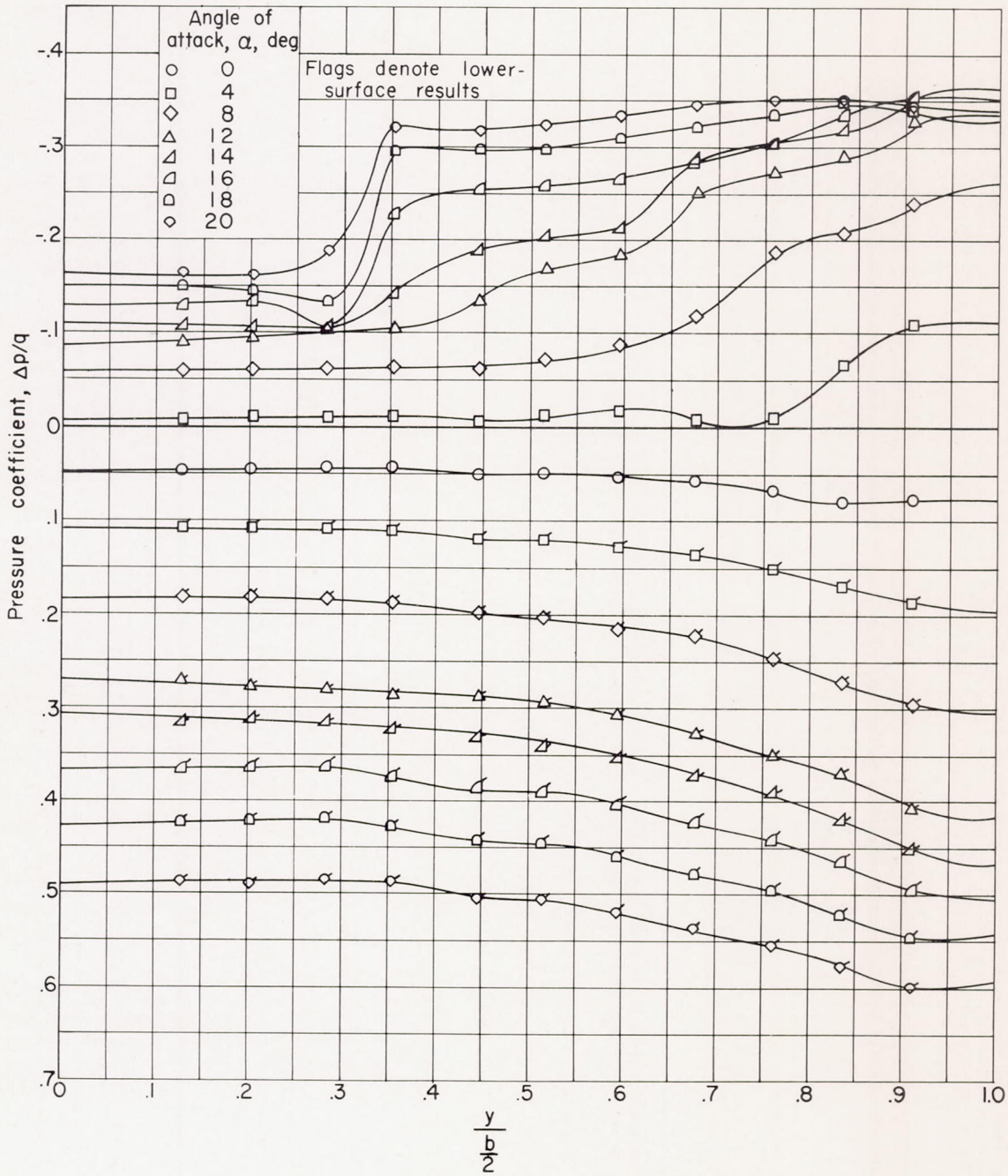

Figure 15.- Spanwise pressure distributions on wing with semiapex angle of 31.75°. Orifices located at 51-percent-chord position.

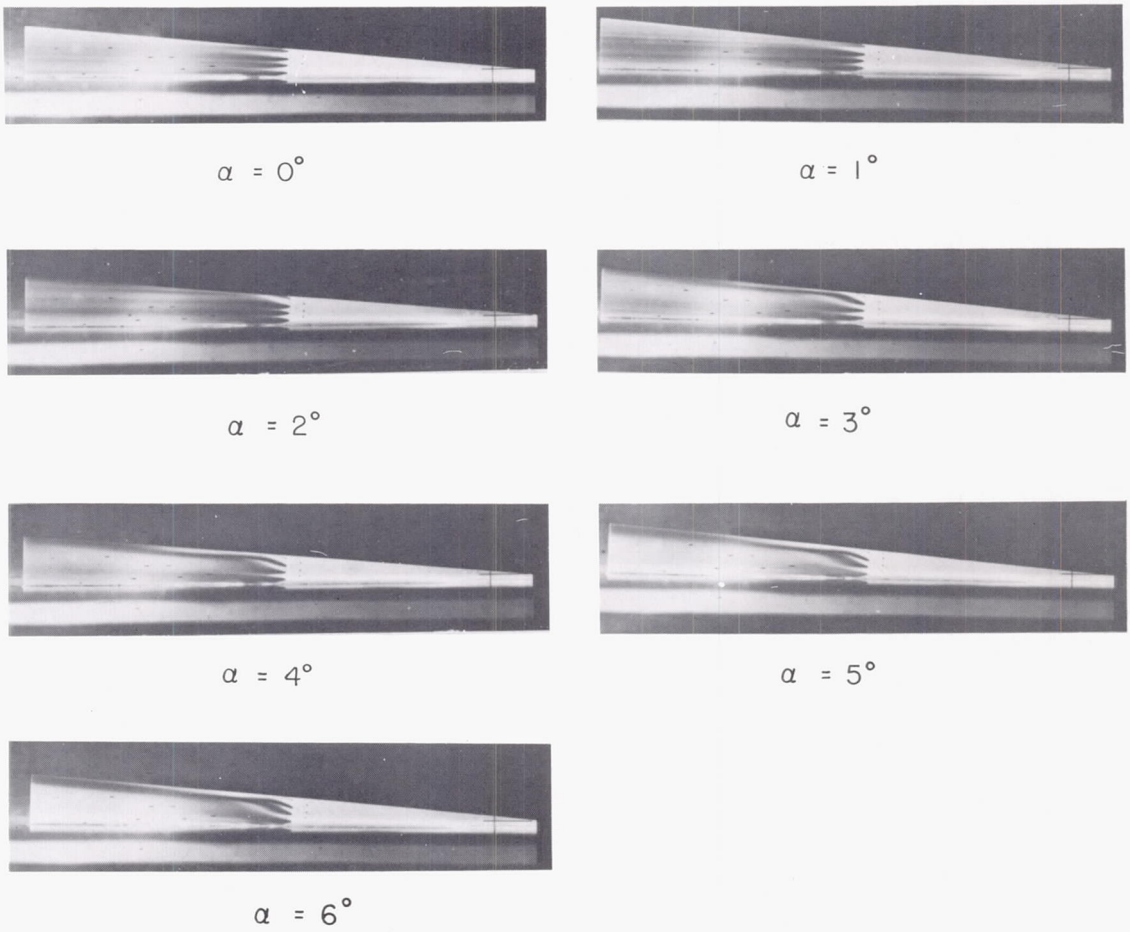

L-89296

Figure 16.- Ink-flow photographs for wing with semiapex angle of 5°.

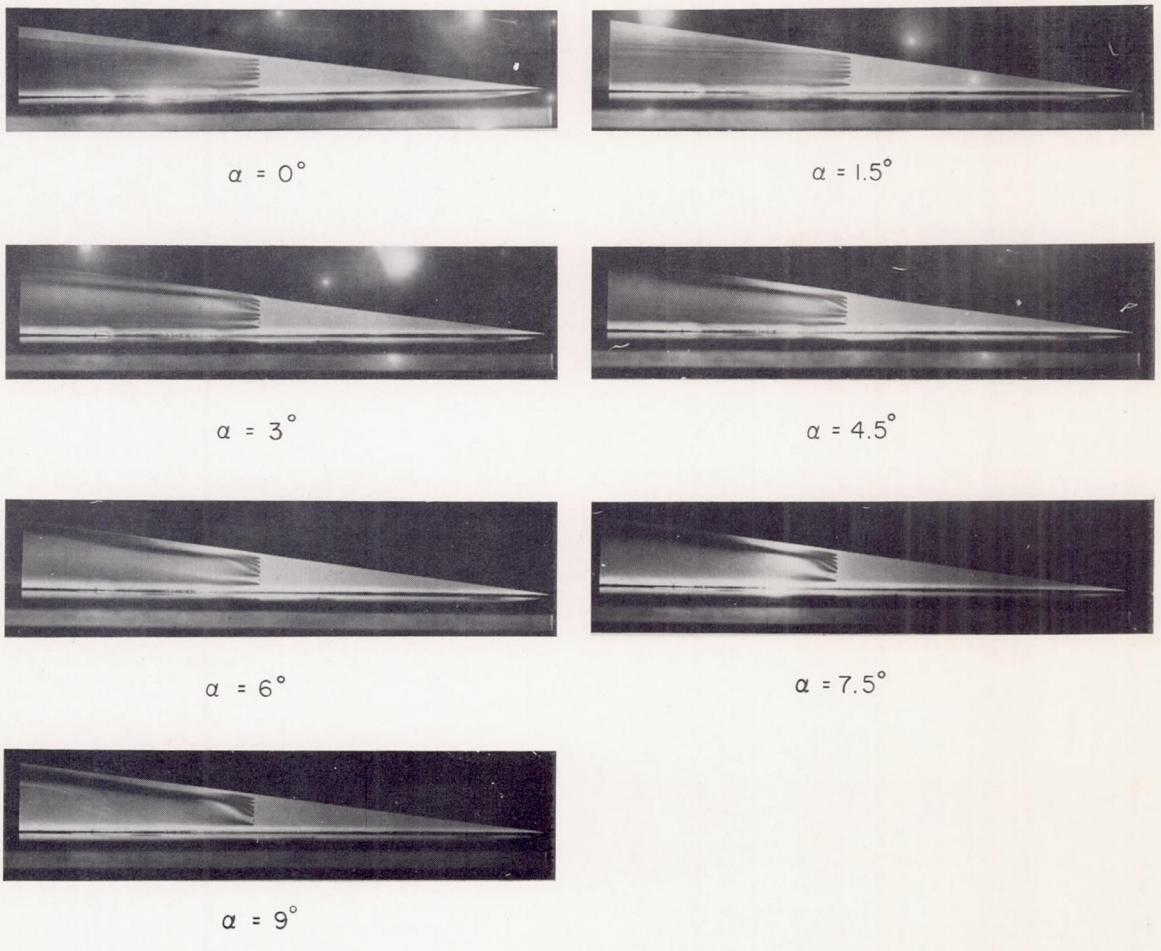

L-89297

Figure 17.- Ink-flow photographs for wing with semiapex angle of 7.5°.

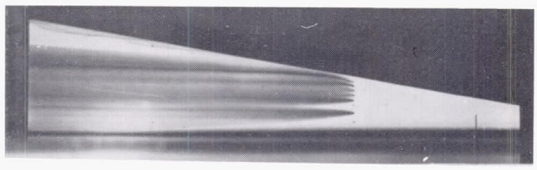

$\alpha = 0°$

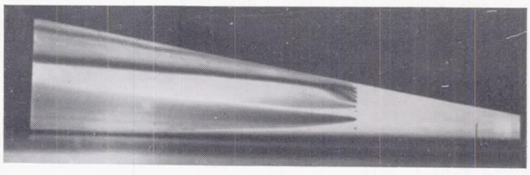

$\alpha = 2°$

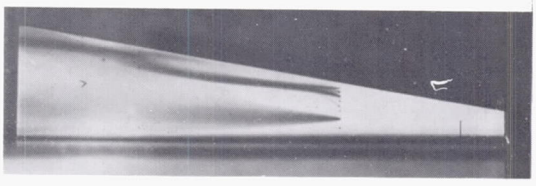

$\alpha = 4°$

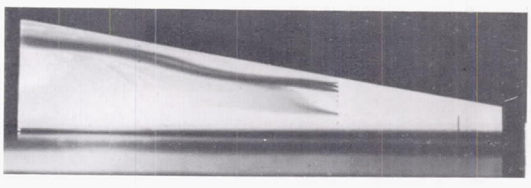

$\alpha = 6°$

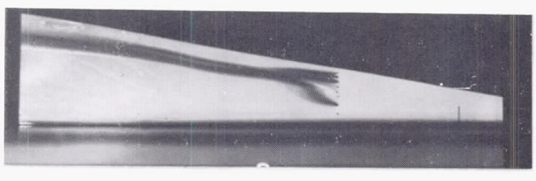

$\alpha = 8°$

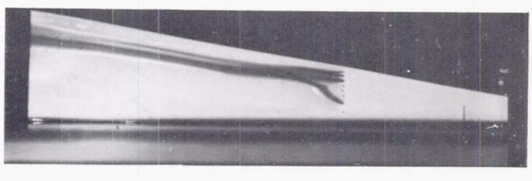

$\alpha = 10°$

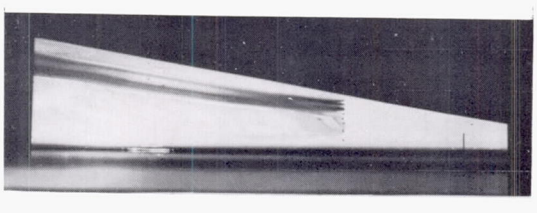

$\alpha = 12°$

L-89298

Figure 18.- Ink-flow photographs for wing with semiapex angle of 10°.

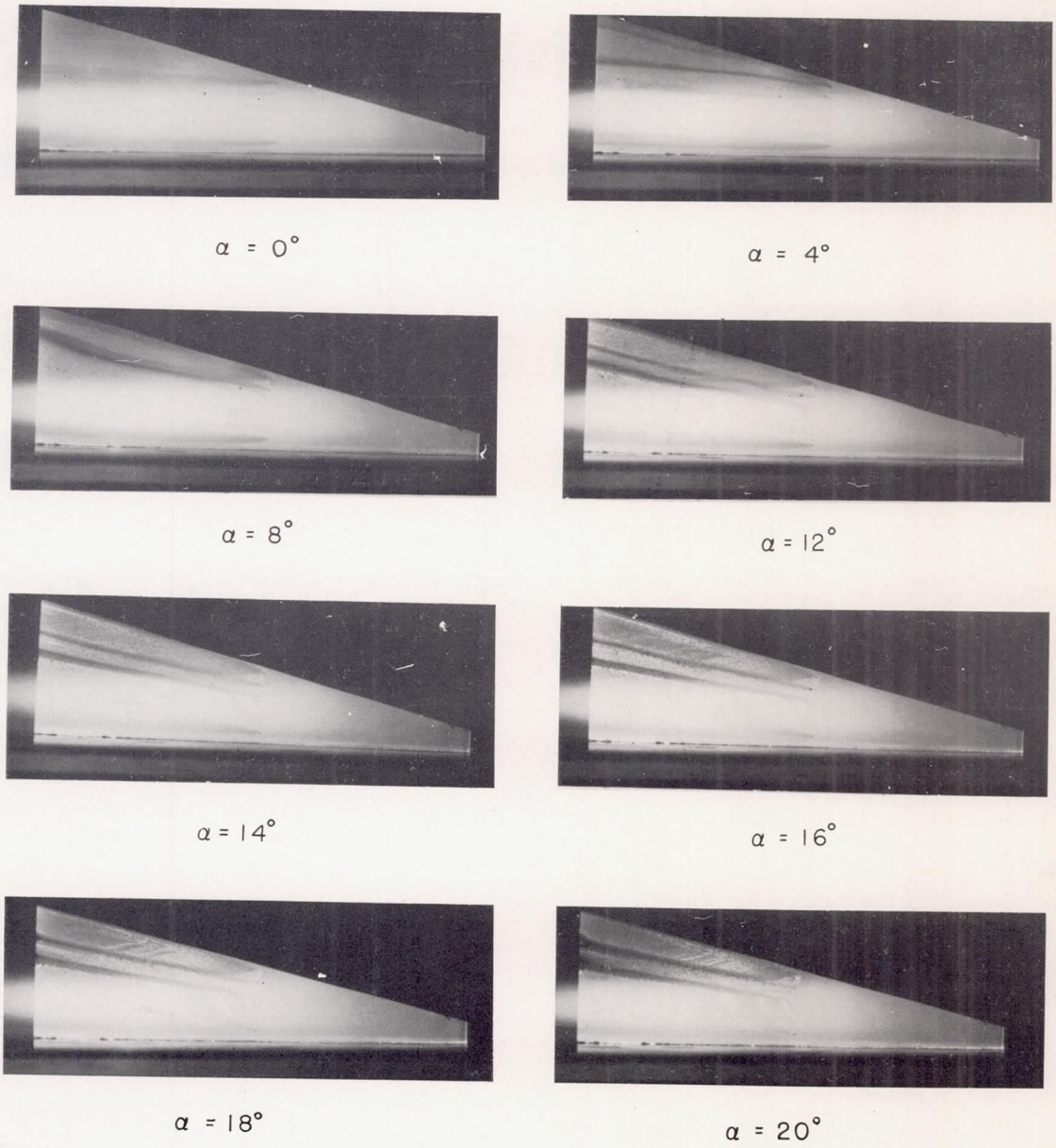

L-89299

Figure 19.- Ink-flow photographs for wing with semiapex angle of 15°.

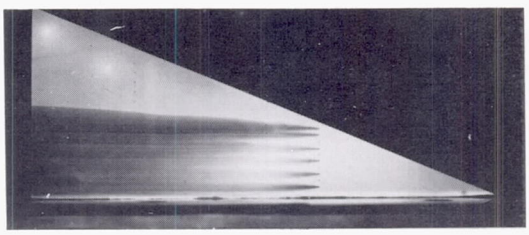

$\alpha = 0°$

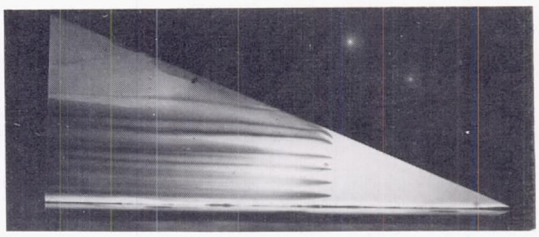

$\alpha = 4°$

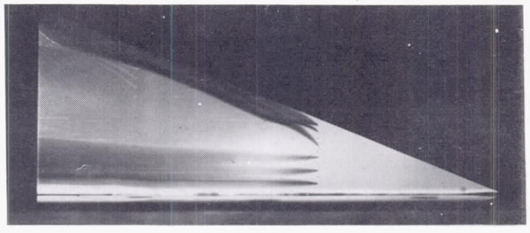

$\alpha = 8°$

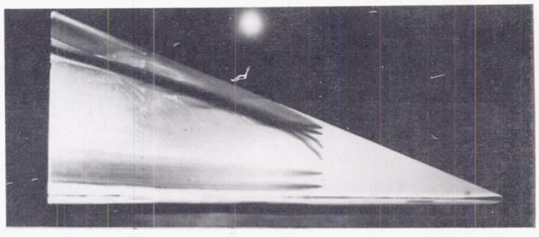

$\alpha = 12°$

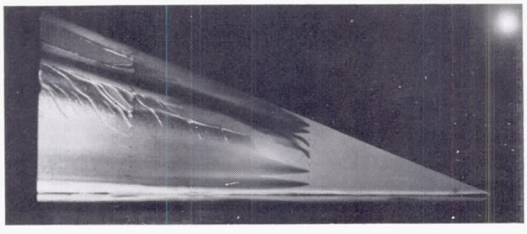

$\alpha = 14°$

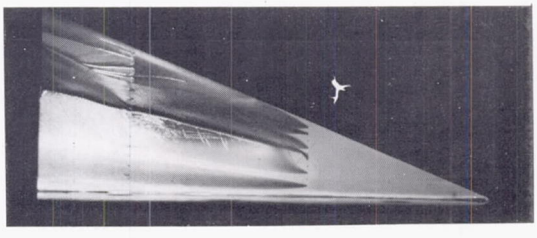

$\alpha = 16°$

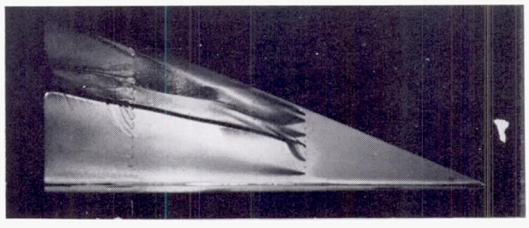

$\alpha = 18°$

L-89300

Figure 20.- Ink-flow photographs for wing with semiapex angle of 22.5°.

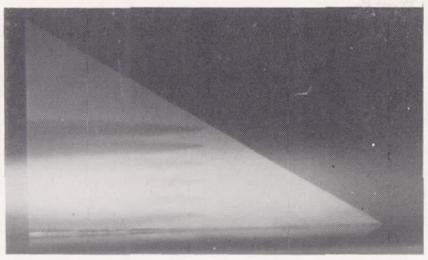

$\alpha = 0°$

$\alpha = 4°$

$\alpha = 8°$

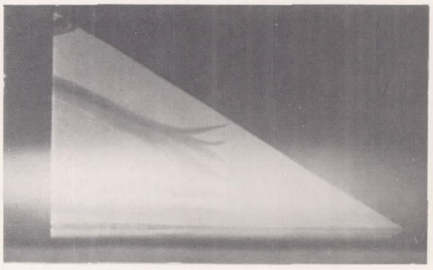

$\alpha = 12°$

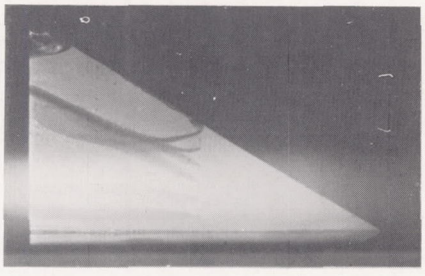

$\alpha = 14°$

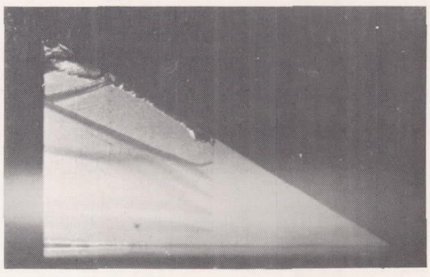

$\alpha = 16°$

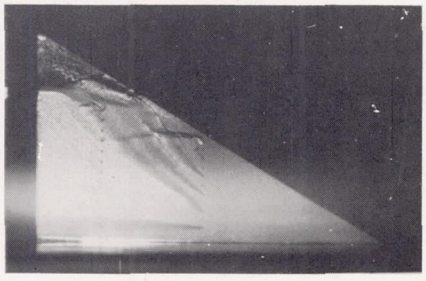

$\alpha = 18°$

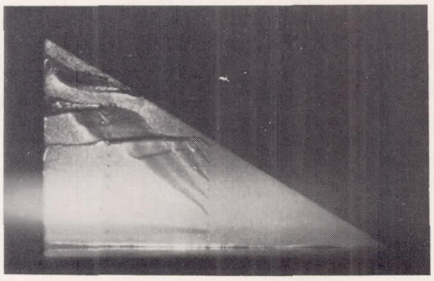

$\alpha = 20°$

L-89301

Figure 21.- Ink-flow photographs for wing with semiapex angle of 31.75°.

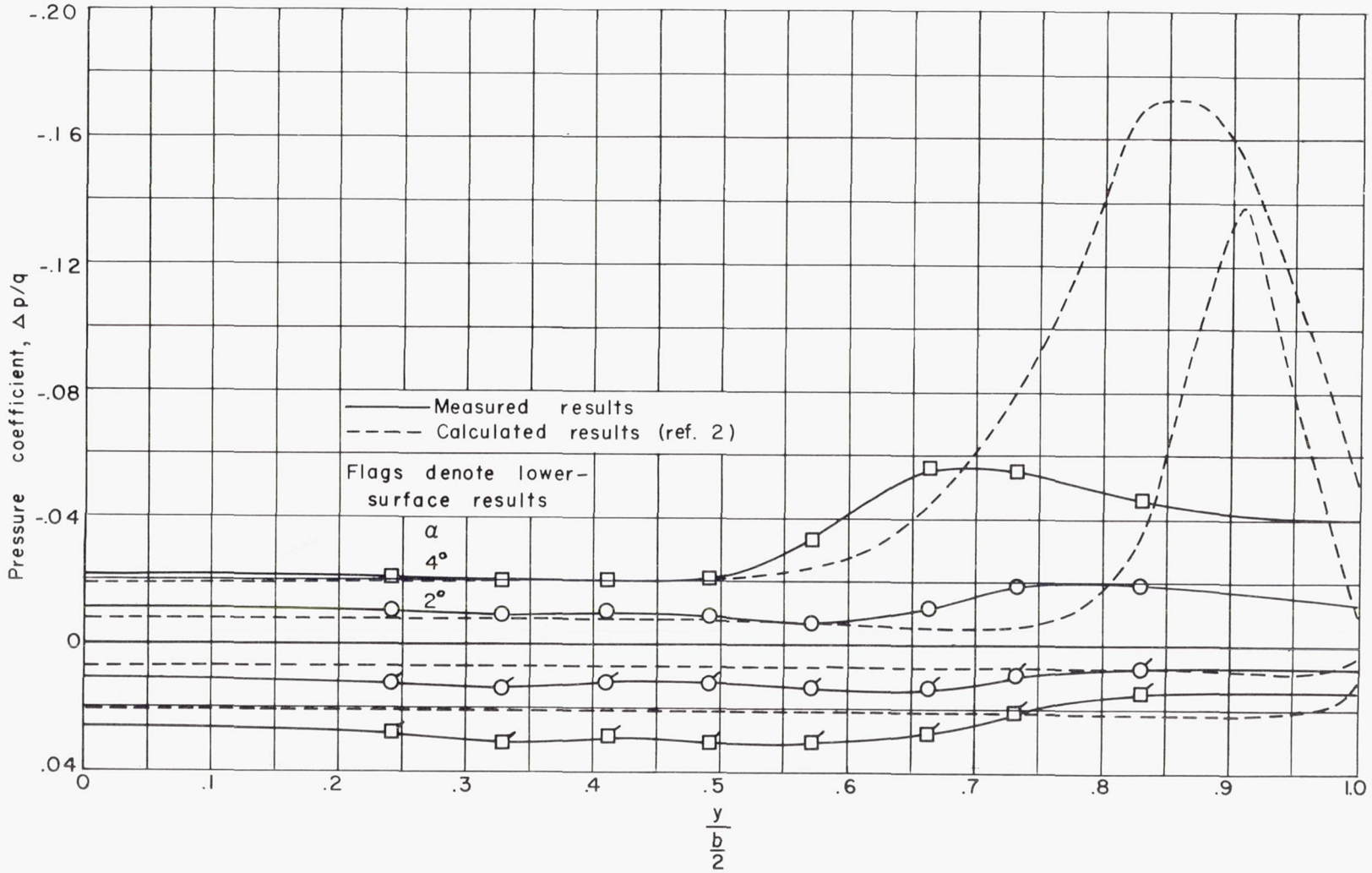

Figure 22.- Comparison of some measured and theoretical pressure distributions. $\epsilon = 5^{\circ}$.